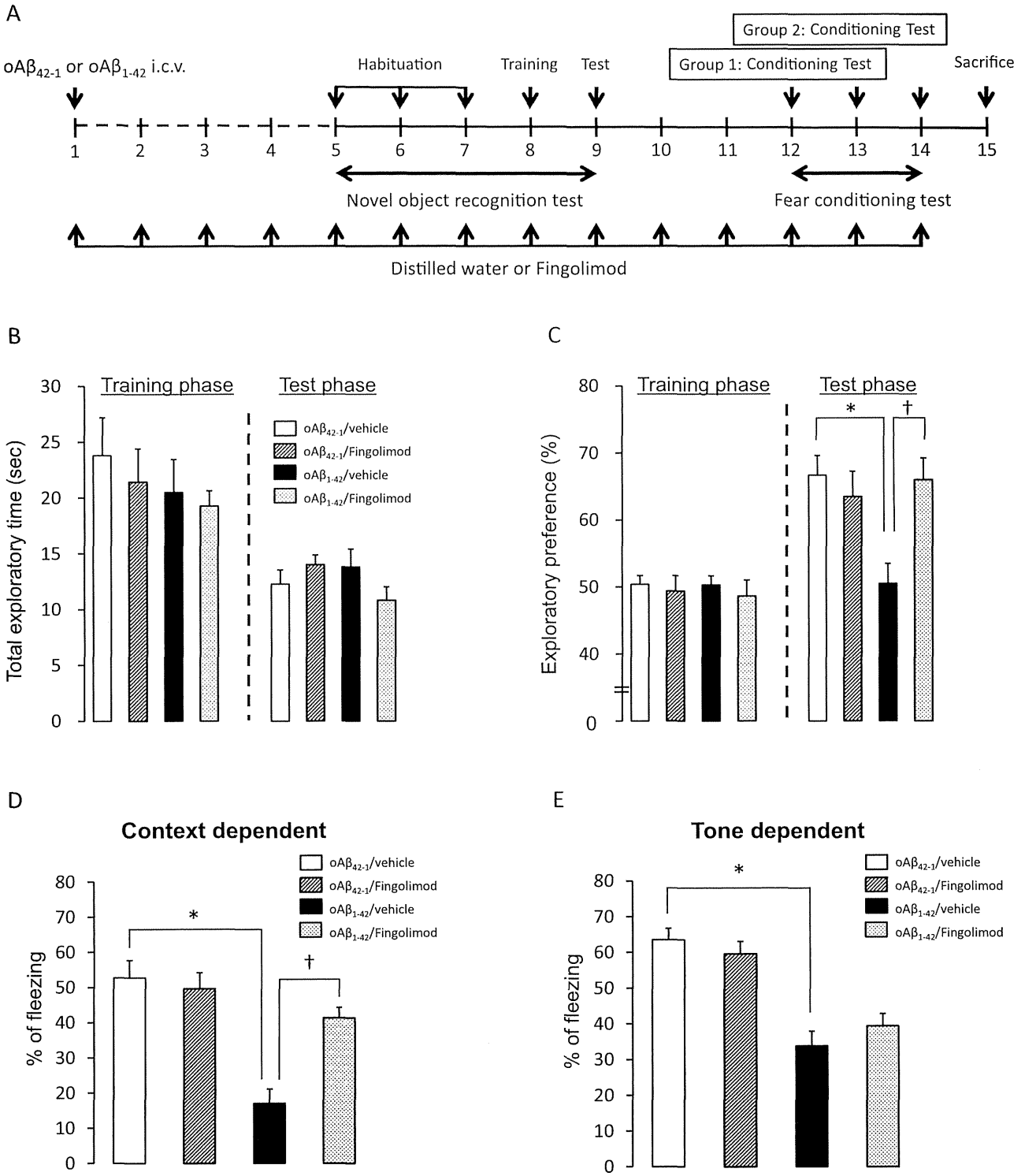

Fig. 1. Oral administration of fingolimod ameliorates oAβ-induced memory impairment.
(A) Experimental scheme of behavioral assessments. (B, C) Effect of fingolimod treatment on object recognition memory of oAβ1-42-injected mice in the novel object recognition test. Retention session was carried out 24 h after training. Values are means ± SE (n = 9–10). *, $p < 0.05$ vs. oAβ42-1/vehicle. †, $p < 0.05$ vs. oAβ1-42/vehicle. (D, E) Effect of treatment with fingolimod on associative learning of oAβ1-42-injected mice in the conditioned-fear learning test. Retention session was carried out 24 h after training. Context-dependent (D) and tone-dependent (E) freezing times were measured. Values are means ± SE (n = 9–10). *, $p < 0.05$ vs. oAβ42-1/vehicle. †, $p < 0.05$ vs. oAβ1-42/vehicle.

14 for group 2). For the contextual test, mice were placed back into the conditioning cage, and the freezing response was measured for 2 min in the absence of the conditioned stimulus. For the cued test, mice were placed in the neutral cage and the freezing response was measured for 1 min in the presence of the conditioned stimulus.

2.5. Quantitative analysis of BDNF protein

Mice were euthanized after the behavioral experiments (days 14 and 15). Contralateral left-brain hemispheres, including the cerebral cortices and hippocampi but excluding the striatum, were

immediately dissected after perfusion of PBS to rule out direct effects of injury induced by the injection needle. Collected samples were immediately frozen and stored at −80 °C until the assay. All dissections were performed using brain matrix (BrainScience Idea, Osaka, Japan) and based on an anatomic atlas [31].

Samples were homogenized in 10 volumes of lysis buffer (137 mM NaCl, 20 mM Tris–HCl [pH 8.0], 1% NP-40, 10% glycerol) with protease inhibitor mixture (Complete, Mini, EDTA-free, Roche) using ultrasonication. After centrifugation at 10,000 × *g* for 15 min at 4 °C, supernatants were assessed using the BDNF ELISA kit (Emax ImmunoAssay Systems; Promega, Madison, WI, USA) as described previously [24]. Assays were carried out in nine or ten independent trials.

2.6. Statistical analysis

All data are expressed as means ± SE. Statistical significance was determined using one-way analysis of variance (ANOVA) for multi-group comparisons. Fisher's LSD was used for post hoc comparison when the *F*-value was significant ($p < 0.05$).

3. Results

3.1. Oral administration of fingolimod ameliorates oAβ-induced memory impairment

Firstly, we investigated the efficacy of fingolimod on oAβ1-42-induced impairment of recognition memory in the NORT. As shown in Fig. 1C, i.c.v. injection of oAβ1-42 significantly reduced exploratory preference for the novel object in the retention session ($F_{(3,35)} = 5.43$, $p < 0.05$), without affecting total exploration time in the training and retention sessions (Fig. 1B, training: $F_{(3,35)} = 0.52$, $p > 0.05$; retention: $F_{(3,35)} = 1.26$, $p > 0.05$), indicating that recognition memory was impaired in oAβ1-42-injected mice. Oral administration of fingolimod (1 mg/kg) in oAβ1-42-injected mice significantly improved exploratory preference in the retention session (Fig. 1C, $F_{(3,35)} = 5.43$, $p < 0.05$), without affecting exploratory preference in the training session (Fig. 1C, $F_{(3,35)} = 0.20$, $p > 0.05$) or total exploration time in the training or retention session (Fig. 1B, training: $F_{(3,35)} = 0.52$, $p > 0.05$; retention: $F_{(3,35)} = 1.26$, $p > 0.05$).

Fingolimod treatment per se had no effect on exploratory preference or total exploration time in oAβ42-1-injected control mice (Fig. 1B and C).

Next, we evaluated associative learning in a conditioned-fear learning test. In the preconditioning phase (training), all groups of mice exhibited very little freezing (data not shown). oAβ1-42-injected mice exhibited less freezing than control mice in both contextual and cued tests (Fig. 1D, context: $F_{(3,35)} = 14.92$, $p < 0.05$; Fig. 1E, tone: $F_{(3,35)} = 16.79$, $p < 0.05$), indicating that associative learning was impaired in oAβ1-42-injected mice. Fingolimod treatment ameliorated the oAβ1-42-induced decrease in the context-dependent freezing response (Fig. 1D: $F_{(3,35)} = 14.92$, $p < 0.05$), but not in the tone-dependent freezing response (Fig. 1E: $p > 0.05$). No alterations of the nociceptive response were found in any group: there was no significant difference between the groups in the minimal current required to elicit flinching/running, jumping, or vocalization (data not shown).

Fingolimod treatment per se had no effect on associative learning in oAβ42-1-injected control mice (Fig. 1D and E).

3.2. Fingolimod restored BDNF production in the brain of oAβ1-42-injected mice.

Finally, we investigated whether fingolimod exerts its neuroprotective effects by up-regulating neuronal BDNF [24].

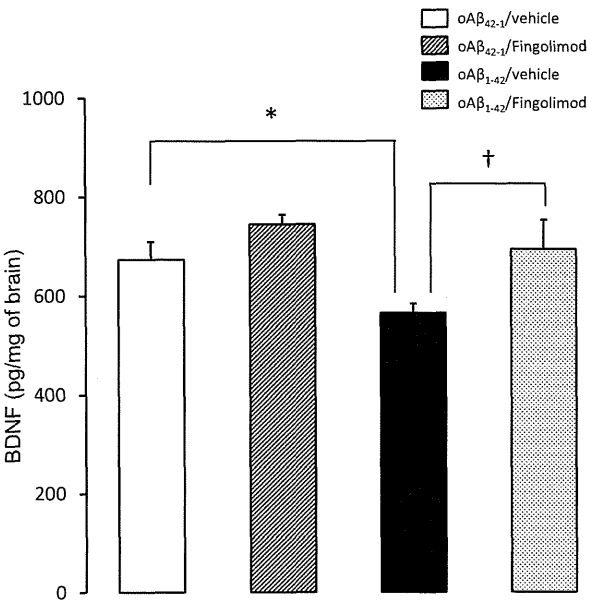

Fig. 2. Fingolimod treatment increased BDNF production in the cerebrum of oAβ1-42-injected mice. Mice were euthanized after behavioral assessments, and BDNF levels in homogenates of cerebral cortices and hippocampi were measured by ELISA. Values are means ± SE ($n = 9$–10). *, $p < 0.05$ vs. oAβ42-1/vehicle. †, $p < 0.05$ vs. oAβ1-42/vehicle.

BDNF levels were reduced in the cerebrum of oAβ1-42-injected mice relative to those in oAβ42-1-injected control mice (Fig. 2, $F_{(3,35)} = 3.91$, $p < 0.05$). Fingolimod treatment restored normal levels of BDNF production in the cerebrum of oAβ1-42-injected mice ($p < 0.05$).

4. Discussion

In this study, we demonstrated that treatment with fingolimod protects against oAβ1-42-induced cognitive impairment, and that this neuroprotection is accompanied by BDNF production.

oAβ injection induced impairment of object-recognition memory (Fig. 1B and C) and associated learning (Fig. 1D and E) in mice. These results are consistent with our previous study revealing the mechanism of Aβ neurotoxicity in this animal model [6]. Oral treatment with fingolimod ameliorated oAβ1-42-induced impairment of recognition memory, and also restored the oAβ1-42-induced decrease in the context-dependent freezing response (Fig. 1D), but did not affect the tone-dependent freezing response (Fig. 1E). In general, context-dependent learning depends on hippocampus function, whereas tone-dependent learning mainly depends on amygdala function. In this animal model, we have shown that cortical and hippocampal extracellular macromolecules are involved in Aβ-induced cognitive impairment and neurotoxicity [6,7,32]. Moreover, it is possible that the expression levels of BDNF and its receptor TrkB are much higher in the hippocampus than in the amygdala [33,34]. Thus, fingolimod may exert its protective effects via inhibition of extracellular macromolecules that induce apoptotic and/or necrotic cell death, or via up-regulation of factors that promote the cell survival and synaptic plasticity in the cortico-hippocampus. Consistent with these findings, fingolimod treatment inhibited neuronal damage in the CA1 or dentate gyrus in rats that received intrahippocampal or intracortical Aβ injection, respectively [35,36].

BDNF/TrkB signaling impacts neuronal survival, axon growth, neuronal transmission, and synaptic plasticity [37–39]. Reduction in the BDNF level leads to disruption of memory formation and maintenance [40,41], whereas overexpression of full-length TrkB

can facilitate spatial memory and associative learning [42]. Moreover, in Alzheimer's disease, the BDNF expression level is severely reduced in the hippocampus and some cortical areas [43,44], and plasma BDNF level might be useful as a behavioral state marker in Alzheimer's disease patients [45,46]. We have also demonstrated that BDNF expression is reduced in the hippocampus in an animal model of mild cognitive impairment [8]. Thus, BDNF signaling is a pivotal modulator of memory formation, and may be involved in the pathology of Alzheimer's disease, which is associated with Aβ production, accumulation, and aggregation [41]. In this study, we showed that repeated treatment with fingolimod restored normal levels of BDNF protein in the cortico-hippocampus of oAβ1-42-injected mice (Fig. 2). Taken together with the results of our previous study showing that BDNF/TrkB signaling is critical for the neuroprotective effects of phosphorylated fingolimod against oAβ-induced neurotoxicity [24], these findings demonstrate that therapeutic effect of fingolimod in Alzheimer's disease is mediated by an increase in neuronal BDNF. Two recent reports have corroborated the potential therapeutic utility of our approach: in one study, fingolimod improved functional recovery after spinal cord injury via nonimmunologic mechanisms [47]; in the other, fingolimod counteracted NMDA-induced neuronal death in a BDNF-dependent manner in a mouse model of Rett syndrome [48]. In addition, S1P itself exerts neuroprotective effects against soluble oAβ-induced cell death, via inactivation of acid sphingomyelinase [49], and fingolimod also reduces neuronal Aβ production via signaling pathways independent of S1PR, although the details remain to be elucidated [50]. Thus, fingolimod may exert neuroprotective effects against oAβ-induced neurotoxicity via multiple pathways.

5. Conclusions

This study demonstrates that fingolimod exerts a striking therapeutic effect in oAβ-induced memory impairment. Thus, S1P receptors and associated signaling pathways are a potential target for the treatment of Alzheimer's disease via up-regulation of BDNF production.

Acknowledgments

This study was supported in part by Novartis Pharm KK; a Grant-in-aid for Scientific Research (No. 25460094) from the Japan Society for the Promotion of Science; a grant from the Takeda Science Foundation; and a grant from the Advanced Research for Medical Products Mining Program of the National Institute of Biomedical Innovation (NIBIO). The funding sources had no involvement in the conduct of the research or preparation of the manuscript.

References

[1] Selkoe DJ, Schenk D. Alzheimer's disease: molecular understanding predicts amyloid-based therapeutics. Annu Rev Pharmacol Toxicol 2003;43:545–84.
[2] Yamada K, Nabeshima T. Animal models of Alzheimer's disease and evaluation of anti-dementia drugs. Pharmacol Ther 2000;88:93–113.
[3] Deshpande A, Mina E, Glabe C, Busciglio J. Different conformations of amyloid beta induce neurotoxicity by distinct mechanisms in human cortical neurons. J Neurosci 2006;26:6011–8.
[4] Doi Y, Mizuno T, Maki Y, Jin S, Mizoguchi H, Ikeyama M. Microglia activated with the toll-like receptor 9 ligand CpG attenuate oligomeric amyloid β neurotoxicity in in vitro and in vivo models of Alzheimer's disease. Am J Pathol 2009;175:2121–32.
[5] De Felice FG, Velasco PT, Lambert MP, Viola K, Fernandez SJ, Ferreira ST. Abeta oligomers induce neuronal oxidative stress through an N-methyl-D-aspartate receptor-dependent mechanism that is blocked by the Alzheimer drug memantine. J Biol Chem 2007;282:11590–601.
[6] Mizoguchi H, Takuma K, Fukuzaki E, Ibi D, Someya E, Akazawa KH, et al. Matrix metalloprotease-9 inhibition improves amyloid beta-mediated cognitive impairment and neurotoxicity in mice. J Pharmacol Exp Ther 2009;331:14–22.
[7] Yamada K, Tanaka T, Han D, Senzaki K, Kameyama T, Nabeshima T. Protective effects of idebenone and alpha-tocopherol on beta-amyloid-(1-42)-induced learning and memory deficits in rats: implication of oxidative stress in beta-amyloid-induced neurotoxicity in vivo. Eur J Neurosci 1999;11:83–90.
[8] Takuma K, Hoshina Y, Arai S, Himeno Y, Matsuo A, Funatsu Y, et al. Ginkgo biloba extract EGb 761 attenuates hippocampal neuronal loss and cognitive dysfunction resulting from chronic restraint stress in ovariectomized rats. Neuroscience 2007;149:256–62.
[9] Brinkmann V, Billich A, Baumruker T, Heining P, Schmouder R, Francis G, et al. Fingolimod (FTY720): discovery and development of an oral drug to treat multiple sclerosis. Nat Rev Drug Discov 2010;9:883–97.
[10] Chun J, Hartung HP. Mechanism of action of oral fingolimod (FTY720) in multiple sclerosis. Clin Neuropharmacol 2010;33:91–101.
[11] Cohen JA, Chun J. Mechanisms of fingolimod's efficacy and adverse effects in multiple sclerosis. Ann Neurol 2011;69:759–77.
[12] Pelletier D, Hafler DA. Fingolimod for multiple sclerosis. N Engl J Med 2012;366:339–47.
[13] Foster CA, Howard LM, Schweitzer A, Persohn E, Hiestand PC, Balatoni B, et al. Brain penetration of the oral immunomodulatory drug FTY720 and its phosphorylation in the central nervous system during experimental autoimmune encephalomyelitis: consequences for mode of action in multiple sclerosis. J Pharmacol Exp Ther 2007;323:469–75.
[14] Adachi K, Kohara T, Nakao N, Arita M, Chiba K, Mishina T, et al. Design, synthesis, and structure-activity relationships of 2-substituted-2-amino-1, 3-propanediols: discovery of a novel immunosuppressant, FTY720. Bioorg Med Chem 1995;5:853–6.
[15] Mandala S, Hajdu R, Bergstrom J, Quackenbush E, Xie J, Milligan J. Alteration of lymphocyte trafficking by sphingosine-1-phosphate receptor agonists. Science 2002;296:346–9.
[16] Matloubian M, Lo CG, Cinamon G, Lesneski MJ, Xu Y, Brinkmann V. Lymphocyte egress from thymus and peripheral lymphoid organs is dependent on S1P receptor 1. Nature 2004;427:355–60.
[17] Pinschewer DD, Ochsenbein AF, Odermatt B, Brinkmann V, Hengartner H, Zinkernagel RM. FTY720 immunosuppression impairs effector T cell peripheral homing without affecting induction, expansion, and memory. J Immunol 2000;164:5761–70.
[18] Brinkmann V. Sphingosine 1-phosphate receptors in health and disease: mechanistic insight from gene deletion studies and reverse pharmacology. Pharmacol Ther 2007;115:84–105.
[19] Brinkmann V, Davis MD, Heise CE, Albert R, Cottens S, Hof R, et al. The immune modulator FTY720 targets sphingosine 1-phosphate receptors. J Biol Chem 2002;277:21453–7.
[20] Dev KK, Mullershausen F, Mattes H, Kuhn RR, Bilbe G, Hoyer D. Brain sphingosine-1-phosphate receptors: implication for FTY720 in the treatment of multiple sclerosis. Pharmacol Ther 2008;117:77–93.
[21] Miron VE, Ludwin SK, Darlington PJ, Jarjour AA, Soliven B, Kennedy TE, Fingolimod. (FTY720) enhances remyelination following demyelination of organotypic cerebellar slices. Am J Pathol 2010;176:2682–94.
[22] Choi JW, Gardell SE, Herr DR, Rivera R, Lee CW, Noguchi K, et al. FTY720 (fingolimod) efficacy in an animal model of multiple sclerosis requires astrocyte sphingosine 1-phosphate receptor 1 (S1P1) modulation. Proc Natl Acad Sci 2011;108:751–6.
[23] Noda H, Takeuchi H, Mizuno T, Suzumura A. Fingolimod phosphate promotes the neuroprotective effects of microglia. J Neuroimmunol 2013;256:13–8.
[24] Doi Y, Takeuchi H, Horiuchi H, Hanyu T, Kawanokuchi J, Jin S, et al. Fingolimod phosphate attenuates oligomeric amyloid β-induced neurotoxicity via increased brain-derived neurotrophic factor expression in neurons. PLoS ONE 2013;8:e61988.
[25] Dahlgren KN, Manelli AM, Stine Jr WB, Baker LK, Krafft GA, LaDu MJ. Oligomeric and fibrillar species of amyloid-beta peptides differentially affect neuronal viability. J Biol Chem 2002;277:32046–53.
[26] Mizuno T, Doi Y, Mizoguchi H, Jin S, Noda M, Sonobe Y, et al. Interleukin-34 selectively enhances the neuroprotective effects of microglia to attenuate oligomeric amyloid-beta neurotoxicity. Am J Pathol 2011;179:2016–27.
[27] Mizoguchi H, Takuma K, Fukakusa A, Ito Y, Nakatani A, Ibi D, et al. Improvement by minocycline of methamphetamine-induced impairment of recognition memory in mice. Psychopharmacology (Berl) 2008;196:233–41.
[28] Takeuchi H, Mizoguchi H, Doi Y, Jin S, Noda M, Liang J, et al. Blockade of gap junction hemichannel suppresses disease progression in mouse models of amyotrophic lateral sclerosis and Alzheimer's disease. PLoS ONE 2011;6:e21108.
[29] Mizoguchi H, Ibi D, Takuma K, Toth E, Sato J, Itohara S, et al. Alterations of emotional and cognitive behaviors in matrix metalloproteinase-2 and -9-deficient mice. Open Behav Sci J 2010;4:19–25.
[30] Mizoguchi H, Yamada K, Nabeshima T. Matrix metalloproteinases contribute to neuronal dysfunction in animal models of drug dependence, Alzheimer's disease, and epilepsy. Biochem Res Int 2011;2011:681385.
[31] Franklin KBJ, Paxinos G. The mouse brain in stereotaxic coordinates San Diego: Academic; 1997.
[32] Tran MH, Yamada K, Olariu A, Mizuno M, Ren XH, Nabeshima T. Amyloid β-peptide induces nitric oxide production in rat hippocampus: association with cholinergic dysfunction and amelioration by inducible nitric oxide synthase inhibitors. FASEB J 2001;15:1407–9.
[33] Conner JM, Lauterborn JC, Yan Q, Gall CM, Varon S. Distribution of brain-derived neurotrophic factor (BDNF) protein and mRNA in the normal adult rat CNS: evidence for anterograde axonal transport. J Neurosci 1997;17:2295–313.
[34] Yan Q, Radeke MJ, Matheson CR, Talvenheimo J, Welcher AA, Feinstein SC. Immunocytochemical localization of TrkB in the central nervous system of the adult rat. J Comp Neurol 1997;378:135–57.

[35] Asle-Rousta M, Kolahdooz Z, Oryan S, Ahmadiani A, Dargahi L. FTY720 (Fingolimod) attenuates beta-amyloid peptide (Aβ42)-induced impairment of spatial learning and memory in rats. J Mol Neurosci 2013;4:1–9.
[36] Hemmati F, Dargahi L, Nasoohi S, Omidbakhsh R, Mohamed Z, Naidu M, et al. Neurorestorative effect of FTY720 in a rat model of Alzheimer's disease: comparison with Memantine. Behav Brain Res 2013;252:415–21.
[37] Drake CT, Milner TA, Patterson SL. Ultrastructural localization of full-length trkB immunoreactivity in rat hippocampus suggests multiple roles in modulating activity-dependent synaptic plasticity. J Neurosci 1999;19:8009–26.
[38] Huang EJ, Reichardt LF. Neurotrophins: roles in neuronal development and function. Annu Rev Neurosci 2001;24:677–736.
[39] Yoshii A, Constantine-Paton M. Postsynaptic BDNF-TrkB signaling in synapse maturation, plasticity, and disease. Dev Neurobiol 2010;70:304–22.
[40] Minichiello L. TrkB signalling pathways in LTP and learning. Nat Rev Neurosci 2009;10:850–60.
[41] Zhang F, Kang Z, Li W, Xiao Z, Zhou X. Roles of brain-derived neurotrophic factor/tropomyosin-related kinase B (BDNF/TrkB) signalling in Alzheimer's disease. J Clin Neurosci 2012;19:946–9.
[42] Koponen E, Voikar V, Riekki R, Saarelainen T, Rauramaa T, Rauramaa T. Transgenic mice overexpressing the full-length neurotrophin receptor trkB exhibit increased activation of the trkB-PLCgamma pathway, reduced anxiety, and facilitated learning. Mol Cell Neurosci 2004;26:166–81.
[43] Ferrer I, Marin C, Rey MJ, Ribalta T, Goutan E, Blanco R. BDNF and full-length and truncated TrkB expression in Alzheimer disease. Implications in therapeutic strategies. J Neuropathol Exp Neurol 1999;58:729–39.
[44] Phillips HS, Hains JM, Armanini M, Laramee GR, Johnson SA, Winslow JW. BDNF mRNA is decreased in the hippocampus of individuals with Alzheimer's disease. Neuron 1991;7:695–702.
[45] Weinstein G, Beiser AS, Choi SH, Preis SR, Chen TC, Vorgas D, et al. Serum brain-derived neurotrophic factor and the risk for dementia: the Framingham Heart Study. JAMA Neurol 2014;71:55–61.
[46] Nagata T, Kobayashi N, Shinagawa S, Yamada H, Kondo K, Nakayama K. Plasma BDNF levels are correlated with aggressiveness in patients with amnestic mild cognitive impairment or Alzheimer disease. J Neural Transm 2014;121:433–41.
[47] Norimatsu Y, Ohmori T, Kimura A, Madoiwa S, Mimuro J, Seichi A. FTY720 improves functional recovery after spinal cord injury by primarily nonimmunomodulatory mechanisms. Am J Pathol 2012;180:1625–35.
[48] Deogracias R, Yazdani M, Dekkers MP, Guy J, Ionescu MC, Vogt KE, Fingolimod. a sphingosine-1 phosphate receptor modulator, increases BDNF levels and improves symptoms of a mouse model of Rett syndrome. Proc Natl Acad Sci USA 2012;109:14230–5.
[49] Gómez-Muñoz A, Kong J, Salh B, Steinbrecher UP. Sphingosine-1-phosphate inhibits acid sphingomyelinase and blocks apoptosis in macrophages. FEBS Lett 2003;539:56–60.
[50] Takasugi N, Sasaki T, Ebinuma I, Osawa S, Isshiki H, Takeo K, et al. FTY720/fingolimod, a sphingosine analogue, reduces amyloid-β production in neurons. PLoS ONE 2013;8:e64050.

Journal of Neuroimmunology 269 (2014) 38–43

Contents lists available at ScienceDirect

Journal of Neuroimmunology

journal homepage: www.elsevier.com/locate/jneuroim

Sirtuin 1 attenuates oxidative stress via upregulation of superoxide dismutase 2 and catalase in astrocytes

Yi Cheng, Hideyuki Takeuchi *, Yoshifumi Sonobe, Shijie Jin, Yue Wang, Hiroshi Horiuchi, Bijay Parajuli, Jun Kawanokuchi, Tetsuya Mizuno, Akio Suzumura

Department of Neuroimmunology, Research Institute of Environmental Medicine, Nagoya University, Furo-cho, Chikusa-ku, Nagoya 464-8601, Japan

ARTICLE INFO

Article history:
Received 9 December 2013
Received in revised form 30 January 2014
Accepted 5 February 2014

Keywords:
Sirtuin 1
Astrocyte
Superoxide dismutase 2
Catalase
Forkhead box protein O4
Reactive oxygen species

ABSTRACT

Sirtuin 1 (SIRT1) exerts a neuroprotective effect on various neurologic diseases. Here we investigated the protective functions of SIRT1 in astrocytes, which are the most abundant cells in the central nervous system. Upregulation of SIRT1 suppressed the expression levels of pro-inflammatory cytokines and increased the expression levels of superoxide dismutase 2 and catalase. Inversely, inhibition of SIRT1 significantly increased the acetylation of forkhead box protein O4, decreased the expression levels of superoxide dismutase 2 and catalase, and increased the production of reactive oxygen species. Our data suggest that astrocytic SIRT1 may elicit neuroprotective effects through its anti-oxidative and anti-inflammatory functions.

1. Introduction

Sirtuin 1 (SIRT1) is a NAD-dependent histone deacetylase involved in induction of lifespan extension by calorie restriction (CR) in many organisms, including yeast, worms, flies, and mice (Kaeberlein et al., 1999; Tissenbaum and Guarente, 2001; Rogina and Helfand, 2004; Morselli et al., 2010). SIRT1 suppresses pro-apoptotic factors and pro-inflammatory factors by downregulating p53 (Vaziri et al., 2001; Solomon et al., 2006) and nuclear factor-kappa B (NF-κB) (Yeung et al., 2004; Chen et al., 2005), whereas it upregulates a select set of proteins related to energy metabolism and pro-survival signals, such as peroxisome proliferator-activated receptor-gamma coactivator 1 alpha (PGC-1α) (Amat et al., 2009; Wareski et al., 2009) and forkhead box class O transcription factors (FOXOs) (van der Horst et al., 2004). PGC-1α, which plays a pivotal role in metabolic regulation, coactivates the peroxisome proliferator-activated receptor transcription factor family and estrogen-related receptors to increase expression of enzymes involved in fatty acid oxidation and oxidative phosphorylation while inhibiting glucose oxidation (Finck & Kelly, 2007). FOXOs play important roles in regulating metabolism, the cell cycle, stress tolerance, and longevity. These transcription factors activate antioxidant enzymes such as superoxide dismutase 2 (SOD2), catalase, or Sestrins to reduce levels of reactive oxygen species (ROS) (Hagenbuchner & Ausserlechner, 2013).

Astrocytes are the most abundant cells in the central nervous system (CNS) and play a crucial role in the maintenance of CNS homeostasis. They cooperate metabolically with neurons in several ways: by supplying metabolites involved in energy production, by aiding in neurotransmitter recycling functions, and by providing antioxidant support (Pastor et al., 2009; Allaman et al., 2011). Astrocytes exert neuroprotective functions during CNS trauma, stroke and cerebrovascular disease, infection, seizure disorders, multiple sclerosis, autoimmune inflammatory disorders, and neurodegenerative disease (Koistinaho et al., 2004; Stevens, 2008; Sofroniew and Vinters, 2010; Ha et al., 2013). Expression of SIRT1 in neurons contributes to neuroprotective functions (Hasegawa & Yoshikawa, 2008; Pizarro et al., 2011; Torres et al., 2011), but the precise roles of astrocytic SIRT1 are still unclear.

In this study, we investigated the roles of astrocytic SIRT1 in anti-inflammatory and anti-oxidant functions. Our findings suggest that astrocytic SIRT1 may be a potential therapeutic target for treatment of neurologic diseases such as multiple sclerosis and Alzheimer's disease.

2. Materials and methods

2.1. Astrocyte culture

The protocols for animal experiments were approved by the Animal Experiment Committee of Nagoya University. Mouse primary astrocytes were prepared from primary mixed glial-cell cultures of newborn C57BL/6J mice (SLC, Shizuoka, Japan), as described previously (Suzumura et al., 1987). The purity of astrocytes was >95%, as determined by immunostaining with anti-GFAP antibody. Cells were cultured in maintenance

* Corresponding author. Tel.: +81 52 789 3883; fax: +81 52 789 5047.
E-mail address: htake@riem.nagoya-u.ac.jp (H. Takeuchi).

http://dx.doi.org/10.1016/j.jneuroim.2014.02.001
0165-5728/

medium (Dulbecco's Modified Eagle Medium supplemented with 10% fetal bovine serum, 5 μg/ml bovine insulin, and 0.6% glucose). Astrocytes were plated at a density of 1×10^4 cells/well in 96-well multidishes, 1×10^5 cells/well in 24-well multidishes, or 5×10^5 cells/well in 6-cm culture dishes.

To assess astrocytic expression of SIRT1, confluent astrocytes were treated with glucose-free medium (Dulbecco's Modified Eagle Medium supplemented with 10% fetal bovine serum and 5 μg/ml bovine insulin) or maintenance medium for 0, 24, 48, or 72 h.

To assess the production of pro-inflammatory cytokines, confluent astrocytes were treated with glucose-free medium containing 1 μg/ml lipopolysaccharide (LPS) and/or 100 nM SIRT1 inhibitor III (Calbiochem) for 72 h.

To measure ROS levels, confluent astrocytes were treated with glucose-free medium containing 1–100 nM SIRT1 inhibitor III for 72 h.

2.2. Quantitative RT-PCR

Total RNA was extracted using the RNeasy Mini kit (Qiagen) and reverse transcribed with SuperScript II (Invitrogen). Expression levels of mRNAs encoding SIRT1, tumor necrosis factor α (TNF-α), interleukin-1β (IL-1β), SOD2, and catalase were evaluated by quantitative PCR (qPCR) using TaqMan Gene Expression Master Mix (Applied Biosystems) on a Rotor-Gene Q real-time PCR cycler (Qiagen). The following mouse gene-specific primers and probes were obtained from Applied Biosystems: SIRT1, Mm00490758_m1; TNF-α, Mm00443258_m1; IL-1β, Mm00434228_m1; SOD2, Mm01313000_m1; catalase, Mm00437992_m1; β-actin, Mm00607939_s1; and GAPDH. Gene expression values were determined by the $\Delta\Delta C_T$ method. The genes of interest were standardized to the geometric mean of β-actin and GAPDH. At least three independent trials were carried out for each assay.

2.3. Immunoprecipitation and immunoblotting

To assess the protein expression levels of SIRT1, SOD2, and catalase, cells were lysed in TNES buffer (50 mM Tris–HCl [pH 7.5], 150 mM NaCl, 1% Nonidet P-40, 2 mM EDTA, and 0.1% SDS) with protease inhibitor mixture (Complete Mini EDTA-free; Roche). Cell lysate proteins dissolved in Laemmli sample buffer (30 μg/well) were separated on 4–20% SDS-polyacrylamide gels (Mini-Protean TGX™, Bio-Rad) and transferred to Hybond-P polyvinylidene difluoride membranes (GE Healthcare). The membranes were blocked with 5% skim milk in Tris-buffered saline containing 0.05% Tween-20 (TBS-T) for 1 h at room temperature, and then incubated overnight at 4 °C with rabbit anti-SIRT1 polyclonal antibody (1:1000, #2028; Cell Signaling Technology), rabbit anti-SOD2 polyclonal antibody (1:200, sc-30080; Santa Cruz Biotechnology), goat anti-catalase polyclonal antibody (1:200, sc-34285; Santa Cruz Biotechnology), goat anti-FOXO4 polyclonal antibody (1:200, sc-5221; Santa Cruz Biotechnology), or mouse anti-β-actin monoclonal antibody (1:5000, AC-15; Sigma), followed by incubation with horseradish peroxidase-conjugated secondary antibodies (1:5000, GE Healthcare) for 1 h at room temperature. To assess FOXO4 acetylation, cells were lysed in TNE buffer (50 mM Tris–HCl [pH 7.5], 150 mM NaCl, 1% Nonidet P-40, 2 mM EDTA) with protease inhibitor mixture, and 500 μg of cell lysate protein was incubated overnight at 4 °C with Dynabeads Protein G (Life Technologies) bound to goat anti-FOXO4 polyclonal antibody. Next, samples were washed three times with TNE buffer and lysed in Laemmli sample buffer. SDS-PAGE and transfer were performed as described above. The membranes were blocked with 5% skim milk in TBS-T for 1 h at room temperature, and then incubated overnight at 4 °C with rabbit anti-acetylated lysine polyclonal antibody (1:1000, #9441; Cell Signaling Technology) or goat

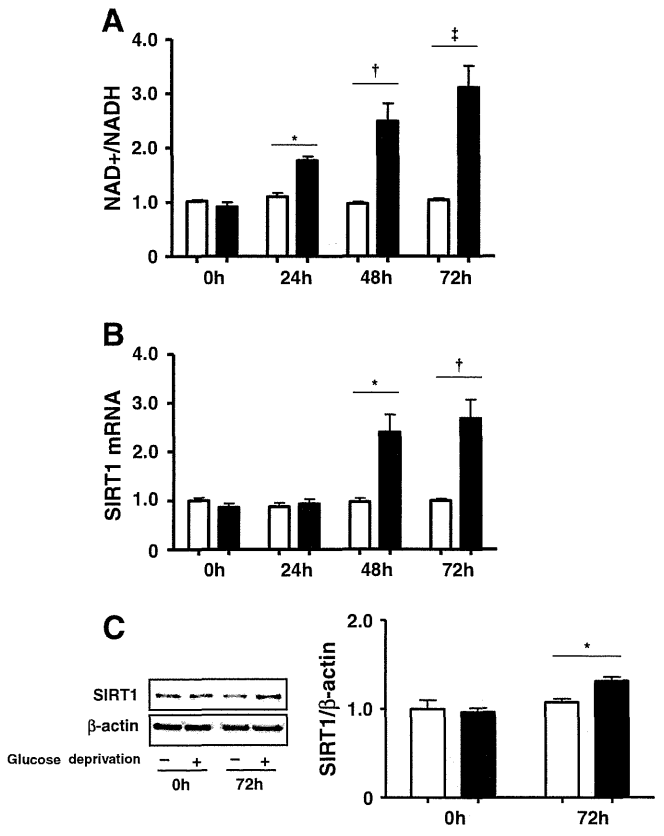

Fig. 1. Glucose deprivation activates the NAD–SIRT1 pathway in astrocytes. Astrocytes were treated with glucose-free medium or maintenance medium for 0, 24, 48, or 72 h. (A) NAD+/NADH ratios (n = 5). *, $p < 0.05$; †, $p < 0.01$; ‡, $p < 0.001$. (B) SIRT1 mRNA levels (n = 3). *, $p < 0.01$; †, $p < 0.001$. (C) SIRT protein levels (n = 4). Left, representative image of immunoblots; right, quantitations of immunoblots. *, $p < 0.01$. White column, control; black column, glucose deprivation. All quantitative data are given as means ± SEM, normalized to the corresponding values from cells in glucose-free medium at 0 h.

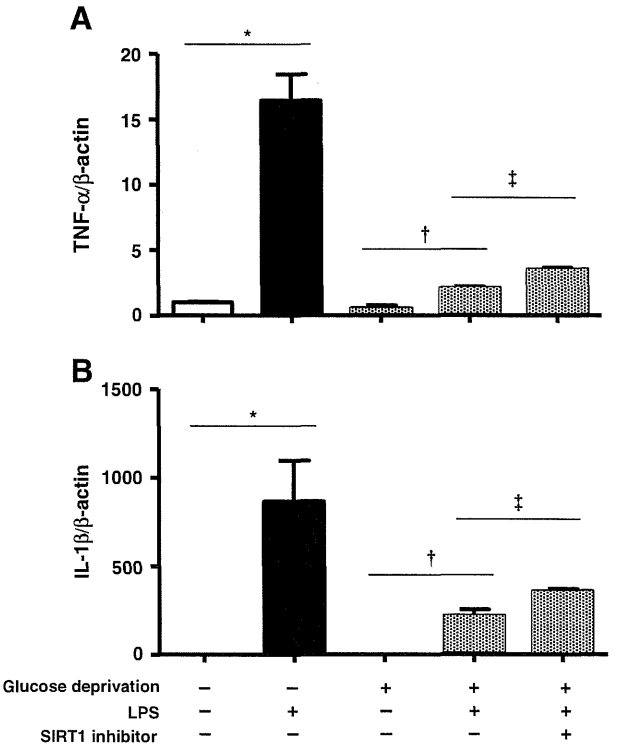

Fig. 2. SIRT1 activation significantly suppresses expression of pro-inflammatory cytokines in astrocytes. Astrocytes were treated with glucose-free medium containing LPS and SIRT1 inhibitor for 72 h. (A) TNF-α mRNA levels. (B) IL-1β mRNA levels. *, $p < 0.05$; †, $p < 0.01$; ‡, $p < 0.001$. Values are means ± SEM (n = 3).

anti-FOXO4 polyclonal antibody (1:200), followed by incubation with horseradish peroxidase-conjugated secondary antibodies (1:5000) for 1 h at room temperature. The signals were visualized using SuperSignal West Dura chemiluminescent substrate (Thermo Fisher Scientific) and quantitated using a CS Analyzer 3.0 system (Atto). Assays were carried out in three independent trials.

2.4. NAD +/NADH quantification

The ratio of NAD + to NADH in astrocytes was determined using the NAD +/NADH Quantification Kit (BioVision).

2.5. Measurement of superoxide and ROS

MitoSOX™ Red mitochondrial superoxide indicator (Invitrogen) was used to detect astrocytic production of superoxide. Live astrocytes were treated with glucose-free medium containing 100 nM SIRT1 inhibitor III (Calbiochem) for 72 h. Cells were incubated with 5 μM MitoSOX™ reagent at 37 °C for 10 min in the dark. After gentle washing and counterstaining with Hoechst 33342, samples were observed using a BZ-8000 deconvolution fluorescence microscope system (Keyence).

To measure ROS, confluent astrocytes on a 96-well plate were treated with glucose-free medium containing 1–100 nM SIRT1 inhibitor III (Calbiochem) for 72 h, and then cells were incubated with 5 μM CellROX™ Deep Red reagent (Invitrogen) at 37 °C for 30 min in the dark. After three gentle washes, the fluorescence at 630/665 nm was measured using a Wallac 1420 $ARVO_{MX}$ (PerkinElmer).

2.6. Statistical analysis

Statistical significance was analyzed with Student's *t*-test or one-way analysis of variance followed by post-hoc Tukey's test, using GraphPad Prism version 5.0 (GraphPad Software).

3. Results

3.1. Glucose deprivation increases the NAD +/NADH ratio and upregulates SIRT1 expression in astrocytes

Calorie restriction strongly induces SIRT1 expression in vivo, and glucose deprivation has been widely used to mimic calorie restriction in vitro. SIRT1 is a NAD-dependent deacetylase, and an increase in the NAD +/NADH ratio upregulates SIRT1 expression (Vaziri et al., 2001). We first sought to determine whether glucose deprivation activates the NAD–SIRT1 pathway in astrocytes. As shown in Fig. 1A, the NAD +/NADH ratio in astrocytes increased significantly, in a time-dependent manner, upon glucose deprivation.

qRT-PCR assessments confirmed that glucose deprivation significantly upregulated SIRT1 mRNA expression in a time-dependent manner (Fig. 1B). The protein level of SIRT1 was also increased by glucose deprivation (Fig. 1C).

3.2. SIRT1 inhibition significantly upregulates astrocytic production of pro-inflammatory cytokines and ROS

We next investigated whether SIRT1 upregulation affects the pro-inflammatory function of astrocytes under pathologic conditions. Whereas LPS stimulation increased the expression levels of pro-inflammatory cytokines such as TNF-α and IL-1β, glucose deprivation dramatically downregulated these cytokines (Fig. 2A and B). The effects of glucose deprivation were partially reversed by the addition of SIRT1 inhibitor (Fig. 2A and B). These data are consistent with those of previous studies (Yeung et al., 2004; Chen et al., 2005).

Next, we investigated whether SIRT1 activation affects ROS production in astrocytes. When astrocytes were deprived of glucose, ROS production did not detectably change (Fig. 3A and B). However, the addition of SIRT1 inhibitor significantly increased ROS production (Fig. 3A and B), whereas treatment with SIRT1 inhibitor did not induce

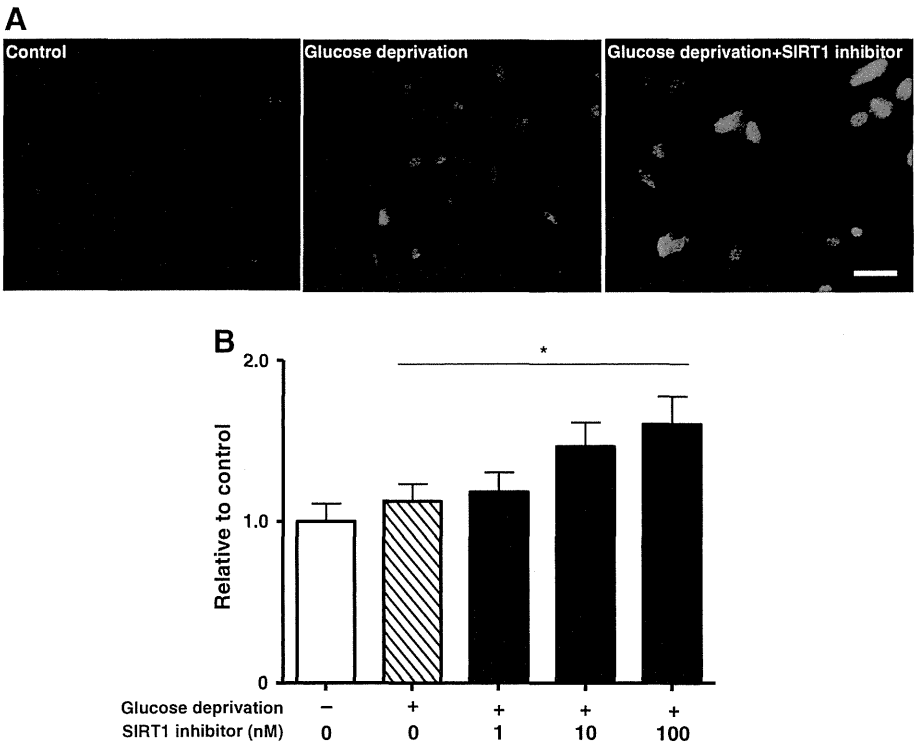

Fig. 3. SIRT1 inhibition significantly upregulates ROS production. ROS production was induced by incubation of astrocytes with SIRT1 inhibitor for 72 h. (A) Representative image of superoxide production in astrocytes. Red, superoxide (MitoSOX™ Red); blue, Hoechst 33342. Scale bar, 30 μm. (B) ROS production in astrocytes. All data were normalized to the control value (white column). *, $p < 0.05$. Values are means ± SEM ($n = 7$).

ROS production under normal glucose condition (data not shown). Previous studies have shown that glucose deprivation also enhances ROS production by mitochondria (Lee et al., 1998; Ouyang & Giffard, 2004). Therefore, glucose deprivation itself induced dual and opposing effects on ROS production, and SIRT1 inhibition revealed the effect of SIRT1 under glucose deprivation. Taken together, these results indicated that SIRT1 is an important negative regulator of inflammation and oxidative stress in astrocytes.

3.3. SIRT1 activation upregulates antioxidant enzymes in astrocytes

SODs and catalase are the main scavengers of ROS. SODs catalyze the conversion of superoxide into oxygen and hydrogen peroxide, which is then converted to oxygen and water by catalase. Mammalian cells express three isoforms of SOD: SOD1, SOD2, and SOD3. Among these three isoforms, SOD1 and SOD2 exert a crucial role in controlling the levels of ROS (Miao & St Clair, 2009).

In order to determine how SIRT1 activation reduced ROS in astrocytes, we examined the expression levels of SOD1, SOD2, and catalase. Glucose deprivation significantly increased the expression levels of SOD2 and catalase; the addition of SIRT1 inhibitor significantly downregulated these proteins (Fig. 4), whereas SOD1 was not affected (data not shown). These data indicated that SOD2 and catalase are the main downstream effectors by which SIRT1 activity suppresses ROS production in astrocytes.

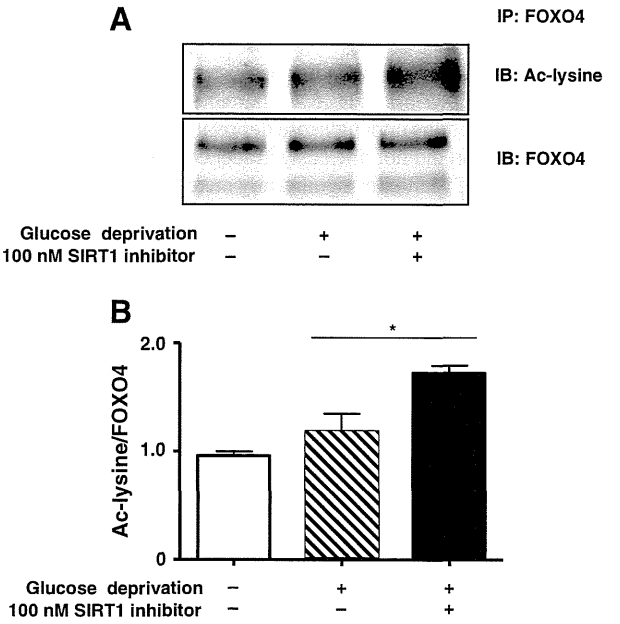

Fig. 5. SIRT1 inhibition increases FOXO4 acetylation. Cell lysates from astrocytes treated with SIRT1 inhibitor for 72 h were immunoprecipitated with anti-FOXO4 antibody and immunoblotted with anti-Ac-lysine antibody and anti-FOXO4 antibody. (A) Representative image of immunoblots. (B) Quantitations of immunoblots. All data were normalized to the control value (white column). *, $p < 0.05$. Values are means ± SEM (n = 3).

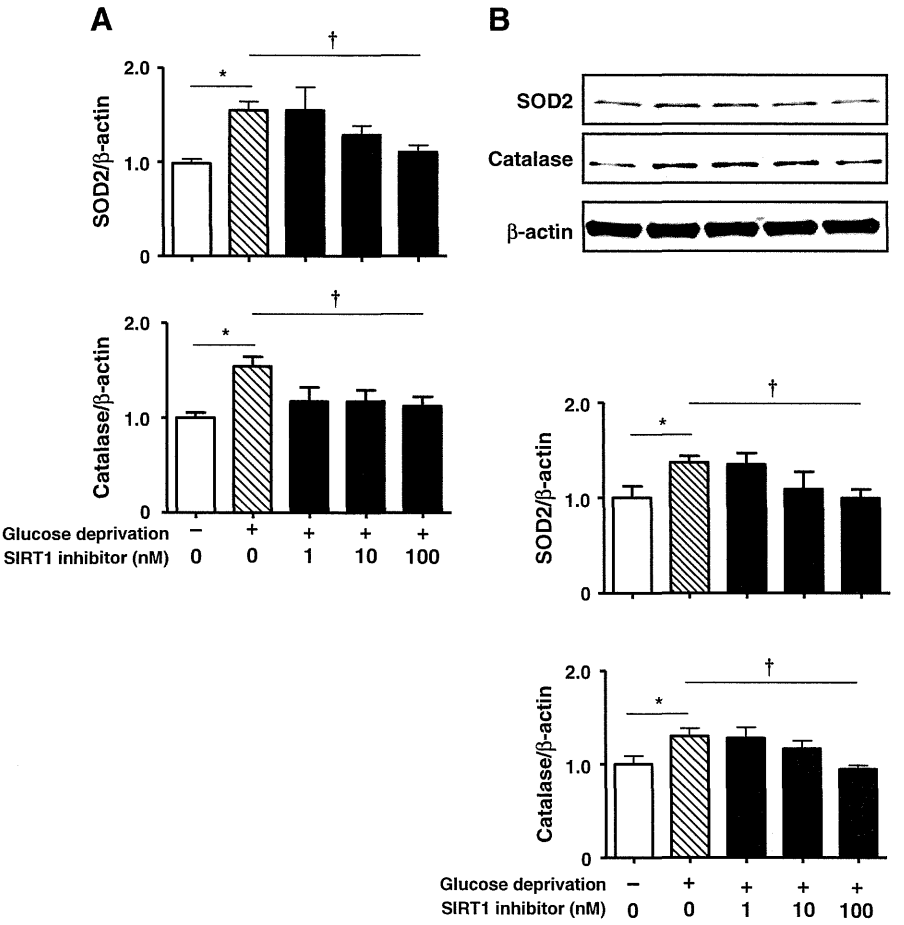

Fig. 4. Glucose deprivation increases SOD2 and catalase expression. Astrocytes were treated with glucose-free medium containing SIRT1 inhibitor for 72 h. (A) SOD2 and catalase mRNA levels. (B) SOD2 and catalase protein levels. Upper panel, representative image of immunoblots; lower panels, quantitations of immunoblots. All data were normalized to the corresponding control values (white column). *, $p < 0.05$; †, $p < 0.01$. Values are means ± SEM (n = 3).

3.4. SIRT1 deacetylates the transcription factor FOXO4

SIRT1 deacetylates histone and non-histone substrates, including PGC-1α, FOXO1, FOXO3a, and FOXO4. Therefore, we examined the acetylation of these proteins under glucose deprivation and SIRT1 inhibition. Glucose deprivation did not obviously influence FOXO4 acetylation, but the addition of SIRT1 inhibitor significantly increased FOXO4 acetylation (Fig. 5). By contrast, SIRT1 did not affect deacetylation of PGC-1α, FOXO1, or FOXO3a (data not shown). Therefore, our data suggested that FOXO4 deacetylation is downstream of SIRT1 in astrocytes.

4. Discussion

In this study, we showed that SIRT1 attenuates oxidative stress and inflammation in astrocytes via upregulation of the antioxidant enzymes SOD2 and catalase. As shown in Fig. 6, signals from calorie restriction increase the NAD+/NADH ratio, leading to upregulation of SIRT1. SIRT1 deacetylates FOXO4, which upregulates SOD2 and catalase activities, leading ultimately to suppression of ROS production.

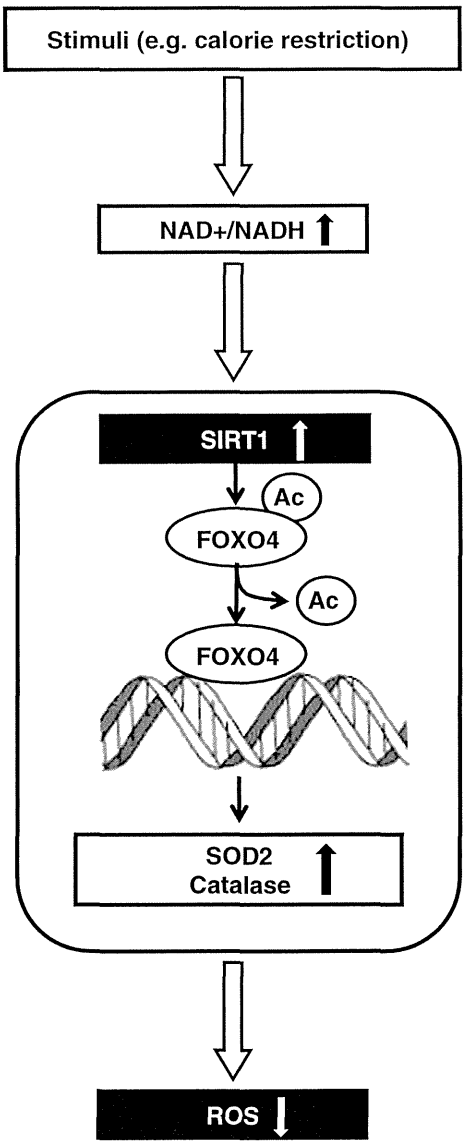

Fig. 6. Proposed mechanism of SIRT1 signaling in astrocytes. Signals from calorie restriction increase the intracellular NAD+/NADH ratio, which subsequently upregulates SIRT1 expression in astrocytes, leading to deacetylation of FOXO4 by SIRT1. Deacetylated FOXO4 binds to the promoter sites of SOD2 and catalase and increases the expression of these antioxidant enzymes, ultimately suppressing ROS production.

SIRT1 can deacetylate a variety of substrates, including PGC-1α (Fernandez-Marcos & Auwerx, 2011), FOXO1 (Potente et al., 2007), FOXO3a (Brunet et al., 2004), and FOXO4 (A van der Horst et al., 2004; Tang, 2010; Armando van der Horst et al., 2004). In glucose-deprived astrocytes, only acetylation of FOXO4 was significantly upregulated by SIRT1 inhibition. Previous studies demonstrated that FOXO4 upregulates the expression levels of SOD2 and catalase by binding to their promoters (Kwon et al., 2010; Araujo et al., 2011). Taken together, our data suggest that SIRT1 plays an important role in the antioxidant defense system via deacetylation of FOXO4, leading to upregulation of SOD2 and catalase.

Elevated ROS levels due to environmental factors can cause significant damage to cells, a situation known as oxidative stress. SIRT1, a crucial cellular survival protein, is also involved in resisting oxidative stress (Salminen et al., 2013): it has been shown to exert an anti-oxidant function in the cardiovascular system (Yang et al., 2013) and kidney (Kitada et al., 2013), but has not yet been demonstrated to do so in the CNS. Excessive ROS production has been implicated in a variety of neurologic disorders such as Alzheimer's disease, Parkinson's disease, and other neurodegenerative diseases, as well as in aging itself. Antioxidant therapies have been proven effective against neuronal damage in these diseases (Uttara et al., 2009). Therefore, our results underscore the potential therapeutic value of astrocytic SIRT1 in protecting against oxidative stress in the CNS.

5. Conclusion

This study demonstrated that SIRT1 suppresses ROS production in astrocytes via deacetylation of FOXO4, leading to upregulation of SOD2 and catalase, suggesting that astrocytic SIRT1 may play a role in neuroprotection by exerting anti-oxidative and anti-inflammatory effects.

Acknowledgments

This work was supported in part by a Grant-in-Aid for Scientific Research on Innovative Areas from the Ministry of Education, Culture, Sports, Science and Technology of Japan; a grant from the Advanced Research for Medical Products Mining Program of the National Institute of Biomedical Innovation (NIBIO) of Japan; and grants from the Ministry of Health, Labour and Welfare of Japan.

References

Allaman, I., Bélanger, M., Magistretti, P.J., 2011. Astrocyte–neuron metabolic relationships: for better and for worse. Trends Neurosci. 34 (2), 76–87. http://dx.doi.org/10.1016/j.tins.2010.12.001.

Amat, R., Planavila, A., Chen, S.L., Iglesias, R., Giralt, M., Villarroya, F., 2009. SIRT1 controls the transcription of the peroxisome proliferator-activated receptor-gamma coactivator-1alpha (PGC-1alpha) gene in skeletal muscle through the PGC-1alpha autoregulatory loop and interaction with MyoD. J. Biol. Chem. 284 (33), 21872–21880. http://dx.doi.org/10.1074/jbc.M109.022749.

Araujo, J., Breuer, P., Dieringer, S., Krauss, S., Dorn, S., Zimmermann, K., et al., 2011. FOXO4-dependent upregulation of superoxide dismutase-2 in response to oxidative stress is impaired in spinocerebellar ataxia type 3. Hum. Mol. Genet. 20 (15), 2928–2941. http://dx.doi.org/10.1093/hmg/ddr197.

Brunet, A., Sweeney, L.B., Sturgill, J.F., Chua, K.F., Greer, P.L., Lin, Y., et al., 2004. Stress-dependent regulation of FOXO transcription factors by the SIRT1 deacetylase. Science (New York, N.Y.) 303 (5666), 2011–2015. http://dx.doi.org/10.1126/science.1094637.

Chen, J., Zhou, Y., Mueller-Steiner, S., Chen, L.-F., Kwon, H., Yi, S., et al., 2005. SIRT1 protects against microglia-dependent amyloid-beta toxicity through inhibiting NF-kappaB signaling. J. Biol. Chem. 280 (48), 40364–40374. http://dx.doi.org/10.1074/jbc.M509329200.

Fernandez-Marcos, P., Auwerx, J., 2011. Regulation of PGC-1a, a nodal regulator of mitochondrial biogenesis. Am. J. Clin. 93, 884–890. http://dx.doi.org/10.3945/ajcn.110.001917.884S.

Finck, B.N., Kelly, D.P., 2007. Peroxisome proliferator-activated receptor gamma coactivator-1 (PGC-1) regulatory cascade in cardiac physiology and disease. Circulation 115 (19), 2540–2548. http://dx.doi.org/10.1161/CIRCULATIONAHA.107.670588.

Ha, S.C., Han, A.R., Kim, D.W., Kim, E.-A., Kim, D.-S., Choi, S.Y., et al., 2013. Neuroprotective effects of the antioxidant action of 2-cyclopropylimino-3-methyl-1,3-thiazoline hydrochloride against ischemic neuronal damage in the brain. BMB Rep. 46 (7), 370–375 (Retrieved from http://europepmc.org/abstract/MED/23884104).

Hagenbuchner, J., Ausserlechner, M.J., 2013. Mitochondria and FOXO3: breath or die. Front. Physiol. 4 (June), 147. http://dx.doi.org/10.3389/fphys.2013.00147.

Hasegawa, K., Yoshikawa, K., 2008. Necdin regulates p53 acetylation via Sirtuin1 to modulate DNA damage response in cortical neurons. J. Neurosci. Off. J. Soc. Neurosci. 28 (35), 8772–8784. http://dx.doi.org/10.1523/JNEUROSCI.3052-08.2008.

Kaeberlein, M., McVey, M., Guarente, L., 1999. The SIR2/3/4 complex and SIR2 alone promote longevity in *Saccharomyces cerevisiae* by two different mechanisms. Gene Dev. 13 (19), 2570–2580.

Kitada, M., Kume, S., Takeda-Watanabe, A., Kanasaki, K., Koya, D., 2013. Sirtuins and renal diseases: relationship with aging and diabetic nephropathy. Clin. Sci. (Lond.) 124 (3), 153–164. http://dx.doi.org/10.1042/CS20120190.

Koistinaho, M., Lin, S., Wu, X., Esterman, M., Koger, D., Hanson, J., et al., 2004. Apolipoprotein E promotes astrocyte colocalization and degradation of deposited amyloid-beta peptides. Nat. Med. 10 (7), 719–726. http://dx.doi.org/10.1038/nm1058.

Kwon, I., Wang, R., Thangaraju, M., Shuang, H., 2010. PKG inhibits TCF signaling in colon cancer cells by blocking β-catenin expression and activating FOXO4. Oncogene 29 (23), 3423–3434. http://dx.doi.org/10.1038/onc.2010.91.PKG.

Lee, Y.J., et al., 1998. Glucose deprivation-induced cytotoxicity and alterations in mitogen-activated protein kinase activation are mediated by oxidative stress in multidrug-resistant human breast carcinoma cells. J. Biol. Chem. 273 (9), 5294–5299. http://dx.doi.org/10.1074/jbc.273.9.5294.

Miao, L., St Clair, D.K., 2009. Regulation of superoxide dismutase genes: implications in disease. Free Radic. Biol. Med. 47 (4), 344–356. http://dx.doi.org/10.1016/j.freeradbiomed.2009.05.018.

Morselli, E., Maiuri, M.C., Markaki, M., Megalou, E., Pasparaki, a, Palikaras, K., et al., 2010. Caloric restriction and resveratrol promote longevity through the Sirtuin-1-dependent induction of autophagy. Cell death Dis. 1 (1), e10. http://dx.doi.org/10.1038/cddis.2009.8.

Ouyang, Y.-B., Giffard, R.G., 2004. Changes in astrocyte mitochondrial function with stress: effects of Bcl-2 family proteins. Neurochem. Int. 45 (2–3), 371–379. http://dx.doi.org/10.1016/j.neuint.2003.07.006.

Pastor, M.D., García-Yébenes, I., Fradejas, N., Pérez-Ortiz, J.M., Mora-Lee, S., Tranque, P., et al., 2009. mTOR/S6 kinase pathway contributes to astrocyte survival during ischemia. J. Biol. Chem. 284 (33), 22067–22078. http://dx.doi.org/10.1074/jbc.M109.033100.

Pizarro, J.G., Verdaguer, E., Ancrenaz, V., Junyent, F., Sureda, F., Pallàs, M., et al., 2011. Resveratrol inhibits proliferation and promotes apoptosis of neuroblastoma cells: role of sirtuin 1. Neurochem. Res. 36 (2), 187–194. http://dx.doi.org/10.1007/s11064-010-0296-y.

Potente, M., Ghaeni, L., Baldessari, D., Mostoslavsky, R., Rossig, L., Dequiedt, F., et al., 2007. SIRT1 controls endothelial angiogenic functions during vascular growth. Gene Dev. 21 (20), 2644–2658. http://dx.doi.org/10.1101/gad.435107.

Rogina, Blanka, Helfand, Stephen L., 2004. Sir2 mediates longevity in the fly through a pathway related to calorie restriction. Proc. Natl. Acad. Sci. 101, 15998–16003.

Salminen, A., Kaarniranta, K., Kauppinen, A., 2013. Crosstalk between oxidative stress and SIRT1: impact on the aging process. Int. J. Mol. Sci. 14 (2), 3834–3859. http://dx.doi.org/10.3390/ijms14023834.

Sofroniew, M.V., Vinters, H.V., 2010. Astrocytes: biology and pathology. Acta Neuropathol. 119 (1), 7–35. http://dx.doi.org/10.1007/s00401-009-0619-8.

Solomon, J.M., Pasupuleti, R., Xu, L., McDonagh, T., Curtis, R., DiStefano, P.S., et al., 2006. Inhibition of SIRT1 catalytic activity increases p53 acetylation but does not alter cell survival following DNA damage. Mol. Cell. Biol. 26 (1), 28–38. http://dx.doi.org/10.1128/MCB.26.1.28-38.2006.

Stevens, B., 2008. Neuron–astrocyte signaling in the development and plasticity of neural circuits. Neuro-Signals 16 (4), 278–288. http://dx.doi.org/10.1159/000123038.

Suzumura, A., Mezitis, S.G., Gonatas, N.K., Silberberg, D.H., 1987. MHC antigen expression on bulk isolated macrophage–microglia from newborn mouse brain: induction of Ia antigen expression by gamma-interferon. J. Neuroimmunol. 15 (3), 263–278 (Retrieved from http://www.sciencedirect.com/science/article/pii/0165572887901214#).

Tang, B.L., 2010. Sirt1 and cell migration. Cell Adhes. Migr. 4 (2), 163–165. http://dx.doi.org/10.4161/cam.4.2.10972.

Tissenbaum, H.A., Guarente, L., 2001. Increased dosage of a sir-2 gene extends lifespan in *Caenorhabditis elegans*. Nature 410, 227–230.

Torres, G., Dileo, J.N., Hallas, B.H., Horowitz, J.M., Leheste, J.R., 2011. Silent information regulator 1 mediates hippocampal plasticity through presenilin1. Neuroscience 179, 32–40. http://dx.doi.org/10.1016/j.neuroscience.2011.01.036.

Uttara, B., Singh, A.V., Zamboni, P., Mahajan, R.T., 2009. Oxidative stress and neurodegenerative diseases: a review of upstream and downstream antioxidant therapeutic options. Curr. Neuropharmacol. 7 (1), 65–74. http://dx.doi.org/10.2174/157015909787602823.

van der Horst, A., Tertoolen, L.G.J., de Vries-Smits, L.M.M., Frye, R.A., Medema, R.H., Burgering, B.M.T., 2004. FOXO4 is acetylated upon peroxide stress and deacetylated by the longevity protein hSir2(SIRT1). J. Biol. Chem. 279 (28), 28873–28879. http://dx.doi.org/10.1074/jbc.M401138200.

Vaziri, H., Dessain, S.K., Ng Eaton, E., Imai, S.I., Frye, R.A., Pandita, T.K., et al., 2001. hSIR2(SIRT1) functions as an NAD-dependent p53 deacetylase. Cell 107 (2), 149–159 (Retrieved from http://www.ncbi.nlm.nih.gov/pubmed/11672523).

Wareski, P., Vaarmann, A., Choubey, V., Safiulina, D., Liiv, J., Kuum, M., et al., 2009. PGC-1 {alpha} and PGC-1{beta} regulate mitochondrial density in neurons. J. Biol. Chem. 284 (32), 21379–21385. http://dx.doi.org/10.1074/jbc.M109.018911.

Yang, Y., Duan, W., Lin, Y., Yi, W., Liang, Z., Yan, J., et al., 2013. SIRT1 activation by curcumin pre-treatment attenuates mitochondrial oxidative damage induced by myocardial ischemia reperfusion injury. Free Radic. Biol. Med. 65, 667–679. http://dx.doi.org/10.1016/j.freeradbiomed.2013.07.007.

Yeung, F., Hoberg, J.E., Ramsey, C.S., Keller, M.D., Jones, D.R., Frye, R.A., et al., 2004. Modulation of NF-kappaB-dependent transcription and cell survival by the SIRT1 deacetylase. EMBO J. 23 (12), 2369–2380.

OPEN

Citation: Cell Death and Disease (2013) 4, e679; doi:10.1038/cddis.2013.198

www.nature.com/cddis

CCL-1 in the spinal cord contributes to neuropathic pain induced by nerve injury

N Akimoto[1,2,5], K Honda[2], D Uta[3], K Beppu[1], Y Ushijima[2], Y Matsuzaki[2], S Nakashima[2], MA Kido[4], K Imoto[3], Y Takano[2] and M Noda*[,1]

Cytokines such as interleukins are known to be involved in the development of neuropathic pain through activation of neuroglia. However, the role of chemokine (C-C motif) ligand 1 (CCL-1), a well-characterized chemokine secreted by activated T cells, in the nociceptive transmission remains unclear. We found that CCL-1 was upregulated in the spinal dorsal horn after partial sciatic nerve ligation. Therefore, we examined actions of recombinant CCL-1 on behavioural pain score, synaptic transmission, glial cell function and cytokine production in the spinal dorsal horn. Here we show that CCL-1 is one of the key mediators involved in the development of neuropathic pain. Expression of CCL-1 mRNA was mainly detected in the ipsilateral dorsal root ganglion, and the expression of specific CCL-1 receptor CCR-8 was upregulated in the superficial dorsal horn. Increased expression of CCR-8 was observed not only in neurons but also in microglia and astrocytes in the ipsilateral side. Recombinant CCL-1 injected intrathecally (i.t.) to naive mice induced allodynia, which was prevented by the supplemental addition of *N*-methyl-D-aspartate (NMDA) receptor antagonist, MK-801. Patch-clamp recordings from spinal cord slices revealed that application of CCL-1 transiently enhanced excitatory synaptic transmission in the substantia gelatinosa (lamina II). In the long term, i.t. injection of CCL-1 induced phosphorylation of NMDA receptor subunit, NR1 and NR2B, in the spinal cord. Injection of CCL-1 also upregulated mRNA level of glial cell markers and proinflammatory cytokines (IL-1β, TNF-α and IL-6). The tactile allodynia induced by nerve ligation was attenuated by prophylactic and chronic administration of neutralizing antibody against CCL-1 and by knocking down of CCR-8. Our results indicate that CCL-1 is one of the key molecules in pathogenesis, and CCL-1/CCR-8 signaling system can be a potential target for drug development in the treatment for neuropathic pain.

Cell Death and Disease (2013) **4**, e679; doi:10.1038/cddis.2013.198; published online 20 June 2013
Subject Category: Neuroscience

Neuropathic pain (also classified as chronic or malignant pain) is associated with nerve injury of multiple aetiology that includes acute trauma, diabetes, cancer, infection and autoimmune pathology.[1] Pathogenesis of neuropathic pain reflects complex remodelling of the spinal cord, with primary role attributed to change of synaptic transmission and activation of neuroglial cells, astrocytes and microglia.[2–4]

Glutamate, the major excitatory neurotransmitter in the brain and spinal cord, exerts its postsynaptic effects via a diverse set of ionotropic and metabotropic membrane receptors. The glutamate ionotropic *N*-methyl-D-aspartate receptors (NMDARs), specifically those localized in the dorsal horn of the spinal cord, are critically involved in nociceptive transmission and synaptic plasticity and have long been considered a target for the treatment of neuropathic pain.[5,6] The native neuronal NMDAR is a tetramer that consists of two NR1 and two NR2 subunits.[7] Phosphorylation of multiple sites in the cytoplasmic C termini of the NR1 and NR2 subunits is known to modulate NMDAR activity and affect synaptic transmission.[8–10]

[1]Laboratory of Pathophysiology, Graduate School of Pharmaceutical Sciences, Kyushu University, 3-1-1 Maidashi, Higashi-ku, Fukuoka 812-8582, Japan; [2]Department of Physiology and Pharmacology, Faculty of Pharmaceutical Sciences, Fukuoka University, 8-19-1 Nanakuma, Jo, Fukuoka 814-0180, Japan; [3]Department of Information Physiology, Division of Neural Signaling, National Institute for Physiological Sciences, 5-1 Higashiyama, Myodaiji, Okazaki 444-8787, Japan and [4]Department of Molecular Cell Biology and Oral Anatomy, Graduate School of Dental Science, Kyushu University, 3-1-1 Maidashi, Higashi-ku, Fukuoka 812-8582, Japan
*Corresponding author: M Noda, Laboratory of Pathophysiology, Graduate School of Pharmaceutical Sciences, Kyushu University, 3-1-1 Maidashi, Higashi-ku, Fukuoka 812-8582, Japan. Tel: +81 92 642 6574; Fax: +81 92 642 6574; E-mail: noda@phar.kyushu-u.ac.jp
[5]Research Fellow of the Japan Society for the Promotion of Science
Keywords: CCL-1; neuropathic pain; glutamate; spinal cord; NMDA receptor
Abbreviations: AMPA, alpha-amino-3-hydroxy-5-methyl-4-isoxazolepropionic acid; AMV, avian myeloblastosis virus; ANOVA, analysis of variance; ATP, adenosine triphospjate; BDNF, brain-derived neurotrophic factor; CCL-1, chemokine (C-C motif) ligand 1; CCL-2, chemokine (C-C motif) ligand 2; CCL-21, chemokine (C-C motif) ligand 21; CCR-8, chemokine (C-C motif) receptor 8; CX3CL-1, chemokine (CX3C motif) ligand 1; DAPI, 4', 6'-diamidino-2-phenylindole, dihydrochloride; DMEM, Dulbecco's modified eagle medium; DRG, dorsal root ganglion; EGTA, ethylene glycol tetraacetic acid; FBS, fetal bovine serum; GABA, γ-amino butyric acid; GFAP, glial fibrillary acid protein; HEPES, 4-(2-hydroxyethyl)-1-piperazineethanesulfonic acid; Iba-1, ionized calcium-binding adapter molecule 1; IC_{50}, half maximal inhibitory kinase; IFN-γ, interferon γ; IL-17, interleukin-17; IL-1β, interleukin 1β; IL-6, interleukin-6; i.t., intrathecal injection; i.p., intraperitoneal injection; L5, lumbar 5; MAPK, mitogen activated protein kinase; MAP2, microtubule-associated protein 2; mEPSC, miniature excitatory postsynaptic current; mRNA, messenger ribo nucleic acid; NeuN, neuron specific nuclear protein; NMDA, N-methyl-D-aspartate; NR1, NMDA receptor 1; NR2B, NMDA receptor 2B; PBS, phosphate buffered saline; pNR1, phosphorylated NR1; pNR2B, phosphorylated NR2B; PSNL, partial sciatic nerve ligation; PVDF, polyvinylidene difluoride; RT-PCR, reverse transcription polymerase chain reaction; SE, standard error; SG neuron, substantia gelatinosa neuron; siRNA, small interfering ribo nucleic acid; sEPSC, spontaneous excitatory postsynaptic current; TCA-3, thymus-derived chemotactic agent 3; TNF-α, tumour necrosis factor-α; TTX, tetrodotoxin; VGAT, vesicular GABA transporter; VGLUT1, vesicular glutamate transport protein 1
Received 11.1.13; revised 03.4.13; accepted 24.4.13; Edited by D Bano

There are many reports that nerve injury triggers reactive changes in peripheral immune system and in neuroglial cells in both peripheral and central nervous systems.[4,11,12] In the periphery, activation of Schwann cells and resident macrophages recruit hematogenous immune cells, which subsequently invade the injured nerves.[12–14] In the spinal dorsal horn receiving the injured sensory afferents, activation of microglia is commonly associated with early establishment stages of neuropathic pain.[2,15,16] Cytokines such as interleukin-1β (IL-1β), tumour necrosis factor-α (TNF-α) and IL-6, which originate from the peripheral injured area or from activated neuroglial cells in the spinal cord, are known to alter synaptic transmission in the dorsal horn.[13,14]

Chemokines and their receptors are widely expressed in immune cells and in the nervous system.[17,18] Recent studies have shown that chemokines C-C motif ligand 2 (CCL-2) and CX3CL-1 induce tactile allodynia (when non-painful innoxious stimuli become painful) through activation of spinal cord microglia.[17,19] These reactive changes mediated through cytokines and chemokines develop in parallel with tactile allodynia, the latter being the main symptom of neuropathic pain.[20]

CCL-1 (also known as thymus-derived chemotactic agent 3) is one of the well-characterized chemokines and is classified into the same CC chemokine group as CCL-2. CCL-1 is secreted by activated T cell, mast cells and endothelial cells and has important role as the chemoattractant for neutrophils and monocytes.[21] Although effects of CCL-1 on the immune cells are well characterized, the roles of CCL-1 in the central nervous system, and especially in the development of neuropathic pain, remain unclear. In this report, we found that CCL-1 is involved in the development of tactile allodynia following peripheral nerve injury through enhancement of spinal nociceptive transmission and activation of glial cells with subsequent release of cytokines.

Results

Expression of CCL-1 in the spinal cord in neuropathic mice. We first examined the development of allodynia in a partial sciatic nerve ligation (PSNL) model. Mice showed a significant increase in withdrawal response to mechanical stimulus in the ipsilateral hind-paw (tactile allodynia) at 7 days after PSNL. The pain score in the ipsilateral hind-paw was 7.5 ± 0.8 ($n=8$), while contralateral hind-paw was 1.9 ± 0.6 ($n=8$) (Figure 1a). In parallel, the protein level of CCL-1 significantly increased 7 days after PSNL in the ipsilateral spinal cord (relative protein level, 0.14 ± 0.01; $n=4$) compared with the contralateral spinal cord (relative protein level, 0.10 ± 0.01; $n=4$) (Figure 1b). On the other hand, levels of other cytokines, TNF-α, interferon-γ and IL-1β

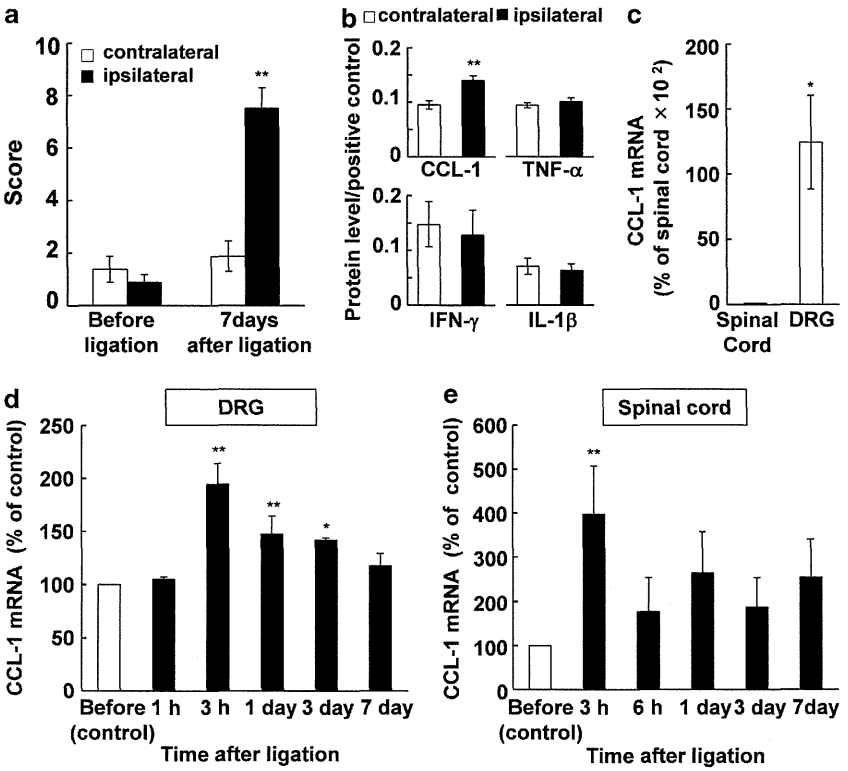

Figure 1 Increase in CCL-1 in the spinal cord after nerve ligation. (**a**) Mice showed tactile allodynia in the ipsilateral hind-paw at 7 days after PSNL. Data represent mean ± S.E. ($n=8$). $^{**}P<0.01$: *versus* before ligation contralateral (two-way analysis of variance (ANOVA) followed by Tukey–Kramer test). (**b**) Cytokine arrays on spinal cord samples at 7 days after nerve ligation. The relative values of cytokine and chemokine proteins were normalized to positive control values in the array Kit. Data represent mean ± S.E. ($n=4$). $^{**}P<0.01$: *versus* contralateral (two-tailed Student's paired *t*-test). (**c**) Comparing CCL-1 mRNA between spinal cord and DRG. Data represent mean ± S.E. ($n=4$). $^{*}P<0.05$: *versus* spinal cord (two-tailed Student's paired *t*-test). (**d**) Time course of CCL-1 mRNA levels in the DRG after nerve ligation was evaluated by quantitative reverse transcriptase (RT)-PCR. (**e**) Time course of CCL-1 mRNA levels in the spinal cord after nerve ligation was evaluated by quantitative RT-PCR. Data represent mean ± S.E. (**d**, $n=4$; **e**, $n=6$). $^{**}P<0.01$, $^{*}P<0.05$: *versus* before ligation (one-way ANOVA followed by Bonferroni test)

were not significantly changed 7 days after nerve ligation (Figure 1b).

Time course of CCL-1 mRNA expression in the spinal cord and dorsal root ganglion (DRG) after nerve ligation. First, we compared CCL-1 mRNA between the spinal cord and DRG before nerve ligation. CCL-1 mRNA was expressed in DRG (12428 ± 3606.7%; $n=4$) more than the spinal cord (Figure 1c). Next, we examined the expression of CCL-1 mRNA in a PSNL model. CCL-1 mRNA level significantly increased at 3 h, 1 and 3 days (194.4 ± 19.9%, 147.3 ± 17.3%, 142.0 ± 2.0%, respectively; $n=4$) after nerve ligation in the DRG (Figure 1d). In the spinal cord, CCL-1 mRNA level significantly increased at 3 h after nerve ligation (361.1 ± 74.5%; $n=6$; Figure 1e).

Time course of CCR-8 protein expression in the spinal cord. CCR-8 is a specific receptor for CCL-1.[22] Nerve ligation increased protein levels of CCR-8 in the ipsilateral dorsal spinal cord 6 h after surgery (Figures 2a and c). The relative protein level of CCR-8 compared with β-actin also showed significant increase at 6 h after ligation (relative protein level, 0.9 ± 0.1; $n=9$; Figure 2b). We performed co-staining of CCR-8 with neuronal or glial markers 6 h after nerve ligation in the spinal cord. Increased expression of CCR-8 was observed not only in neurons but also in microglia and astrocytes in the ipsilateral side (Figure 3). In addition, we showed that CCR-8 was expressed not only on glutamatergic neurons but also on GABAergic neuronal fibers in primary cultured neurons (Supplementary Figure S1).

Injection of a neutralizing antibody against CCL-1 inhibited nerve ligation-induced allodynia. To examine the prophylactic effect of blocking CCL-1 against tactile allodynia, a neutralizing antibody against CCL-1 (anti-CCL-1, 2.5, 25 and 50 ng) was injected i.t. 10 min before nerve ligation and for 6 consecutive days after nerve ligation. The injection of 50 ng anti-CCL-1 antibody significantly reduced tactile allodynia in 3, 5 and 7 days after nerve ligation (pain score at each time point, 5.2 ± 0.8, 6.0 ± 0.8 and 6.0 ± 0.9; $n=15$, respectively; Figure 4a). The inhibition by prophylactic administration of anti-CCL-1 antibody was concentration-dependent (Figure 4b). In order to test the effects of post-chronic administration, daily injection of anti-CCL-1 antibody was started 3 days after nerve ligation and continued for 7 days. Unlike prophylactic administration, the tactile allodynia was not blocked once it was induced by nerve ligation (Figure 4c).

Injection of CCL-1 induced allodynia, which was attenuated by NMDAR inhibitor. We next examined the

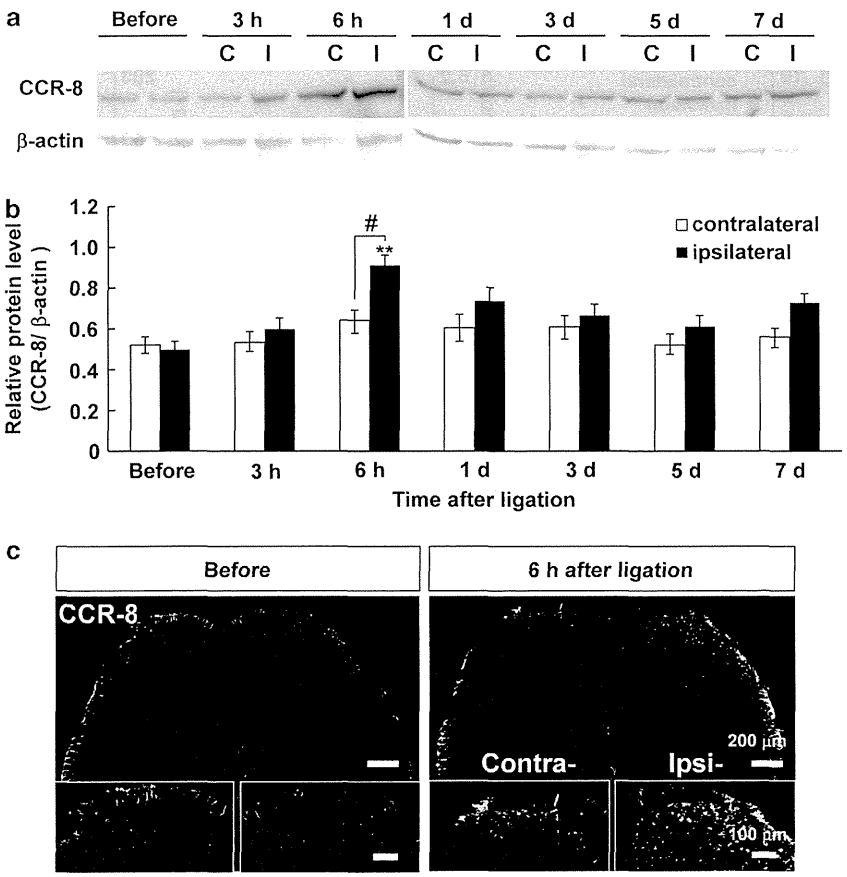

Figure 2 Expression of CCR-8 in the spinal cord following nerve ligation. (**a** and **b**) Protein levels of CCR-8, a selective receptor for CCL-1, in the spinal cord at different time points after nerve ligation were evaluated by western blotting. C, contralateral;I, ipsilateral. Data represent mean ± S.E. (**b**, $n=9$). $^{**}P<0.01$: *versus* ipsilateral before ligation, $^{\#}P<0.05$: *versus* contralateral (two-way analysis of variance followed by Tukey–Kramer tests). (**c**) Immunostaining for CCR-8 in contralateral (Contra-) and ipsilateral (Ipsi-) spinal cord before and 6 h after nerve ligation. Bars = 200 μm (upper panels), 100 μm (lower panels)

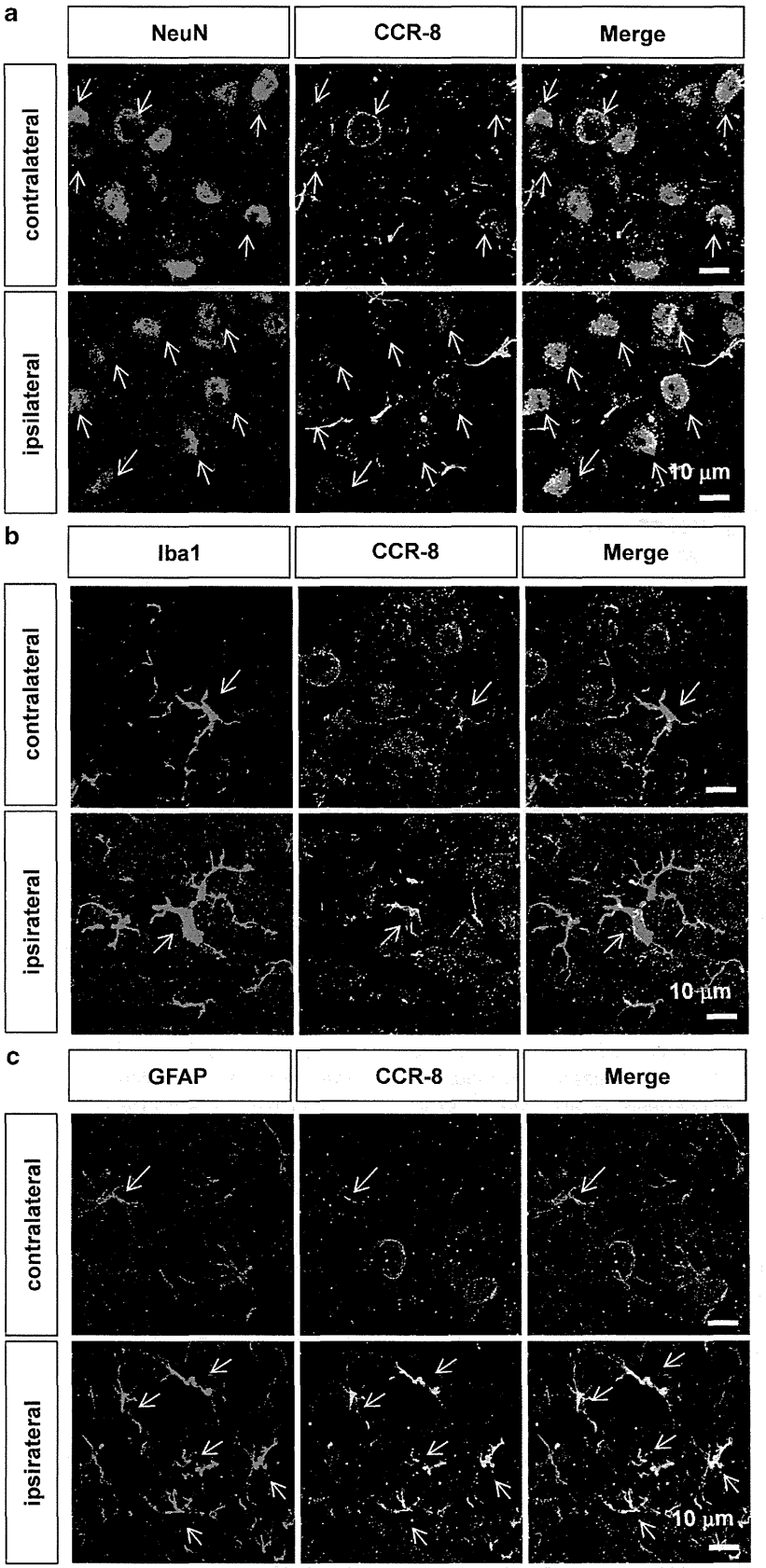

Figure 3 CCR-8 expression in neurons, microglia and astrocytes after nerve ligation. (**a**) Immunostaining for NeuN (red) and CCR-8 (green) 6 h after nerve ligation in the spinal cord. Bars = 10 μm. (**b**) Immunostaining for Iba1 (red) and CCR-8 (green) 6 h after nerve ligation in the spinal cord. Bars = 10 μm. (**c**) Immunostaining for GFAP (red) and CCR-8 (green) 6 h after nerve ligation in the spinal cord. Bars = 10 μm

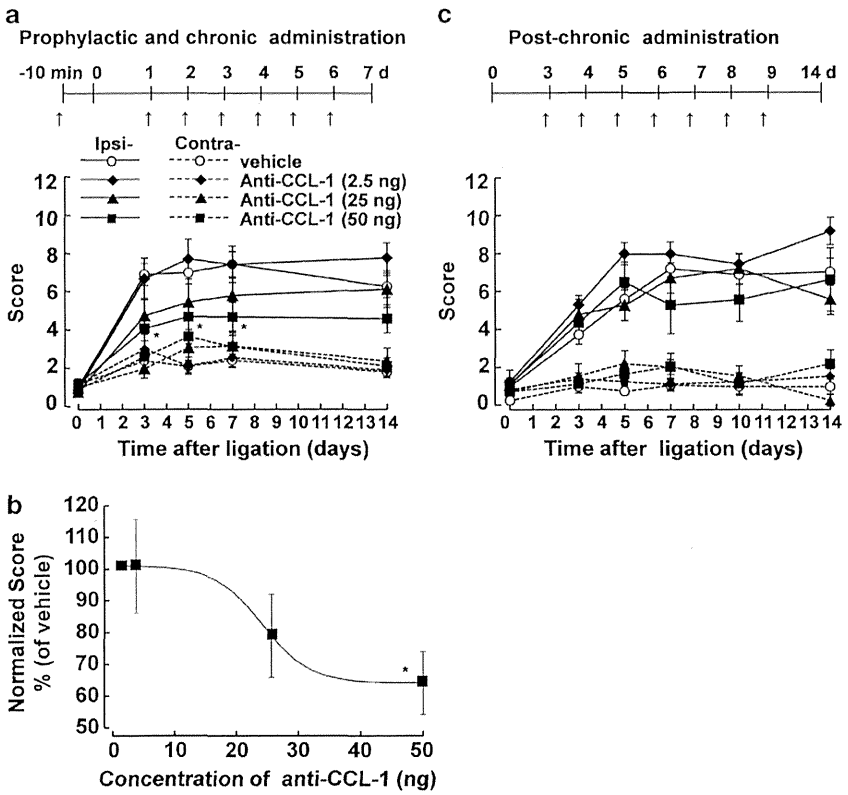

Figure 4 Inhibition of ligation-induced allodynia by neutralizing antibody against CCL-1. (**a** and **c**) Effects of CCL-1 neutralizing antibody (anti-CCL-1) on allodynia induced by nerve ligation. CCL-1 neutralizing antibody (anti-CCL-1) or vehicle (control serum) was first injected 10 min before nerve ligation (**a**) or 3 days after nerve ligation (**c**), followed by daily administration (shown by arrows). Scores were measured using a von Frey filament (vehicle, $n=17$; each concentration of anti-CCL-1, $n=15$). 0 = before ligation. (**b**) Concentration-dependent inhibition of allodynia by anti-CCL-1 antibody 7 days after nerve ligation by the method of prophylactic and chronic administration. Each data represent mean ± S.E. $^*P<0.05$: *versus* vehicle (two-way analysis of variance followed by Tukey–Kramer test)

effect of an intrathecal (i.t.) injection of CCL-1 on nociceptive behaviour. The effect of CCL-1 was dose- and time-dependent; 25 ng CCL-1 significantly increased the pain score after 10, 20, 30, 40 and 80 min (pain score at each time point, 8.6 ± 1.2, 11.3 ± 1, 11.4 ± 1.7, 11.6 ± 0.9, 9.2 ± 1.4 and 7.4 ± 0.9, respectively; $n=8$; Figure 5a). The pain score 20 min after i.t. injection of different concentration of CCL-1 is presented in Figure 5b. NMDARs are critical in pathogenesis of allodynia.[5,6] In our model, the allodynia induced by i.t. injection of CCL-1 (25 ng) was dose-dependently blocked by co-injection of MK-801, a non-competitive use-dependent NMDAR antagonist, at concentration of 125, 250 and 500 pM (Figure 5c). MK-801 showed dose-dependent inhibition of allodynia induced by CCL-1 at 10, 20, 30, 40 and 50 min after injection (pain score at each time point, 3.0 ± 0.7, 4.6 ± 0.7, 6.4 ± 1.0, 4.3 ± 0.8, 4.0 ± 0.7, respectively; $n=8$; Figure 5c). The IC_{50} for MK-801 effects was 354 pM ($n=8$) when determined in 20 min after i.t. injection of CCL-1 (Figure 5d), suggesting the role of NMDA-mediated transmission in allodynia.

CCL-1 increased glutamate release in the superficial dorsal horn of the spinal cord. We examined the action of CCL-1 on excitatory synaptic transmission in the superficial spinal dorsal horn, in the substantia gelatinosa (lamina II), by using whole-cell patch-clamp recordings from mouse spinal cord slices. When holding the cell at −70 mV, substantia gelatinosa neurons exhibited spontaneous excitatory postsynaptic currents (sEPSCs) with average frequency of 7.1 ± 1.0 Hz and amplitude of 11.4 ± 0.9 pA ($n=9$). In four of the nine cells examined, bath application of CCL-1 (50 ng/ml) for 60–90 s enhanced the excitatory synaptic transmission as shown in Figure 5e; this action lasted for more than 3–5 min. In the CCL-1-sensitive cells, the frequency and amplitude of sEPSCs in the presence of CCL-1 were 174 ± 11% and 110 ± 6.3% of controls, respectively (Figure 5e). In the presence of TTX (1 μM), such excitatory effect of CCL-1 was also detected in two out of the six cells tested (data not shown).

NMDAR phosphorylation after injection of CCL-1 in the spinal cord. We examined whether CCL-1 induced phosphorylation of NR1 and NR2B subunits of NMDAR in the spinal cord using western blotting (Figures 6a and b). CCL-1 affected phosphorylation levels of NR1 subunit at Ser896 (p-NR1) in the spinal cord at 3 h, 1 and 3 days after injection of CCL-1 (25 ng, i.t.) (relative protein levels, 2.7 ± 0.75, 4.5 ± 1.16, 3.5 ± 0.88, respectively; $n=3$; Figure 6c). After immunoblotting, the membrane was stripped and reprobed with anti-NR1 antibody (Figure 6a). However, CCL-1 had no effect on the increase of NR1 protein level (Figure 6d). The protein level of p-NR1/NR1 was increased at 1, 3 h, 1 and 3 days after injection of CCL-1 (25 ng, i.t.) (relative protein levels, 5.5 ± 0.69, 5.5 ± 1.32, 9.8 ± 1.84, 7.3 ± 1.46, respectively; $n=3$; Figure 6e). CCL-1 induced phosphorylation of

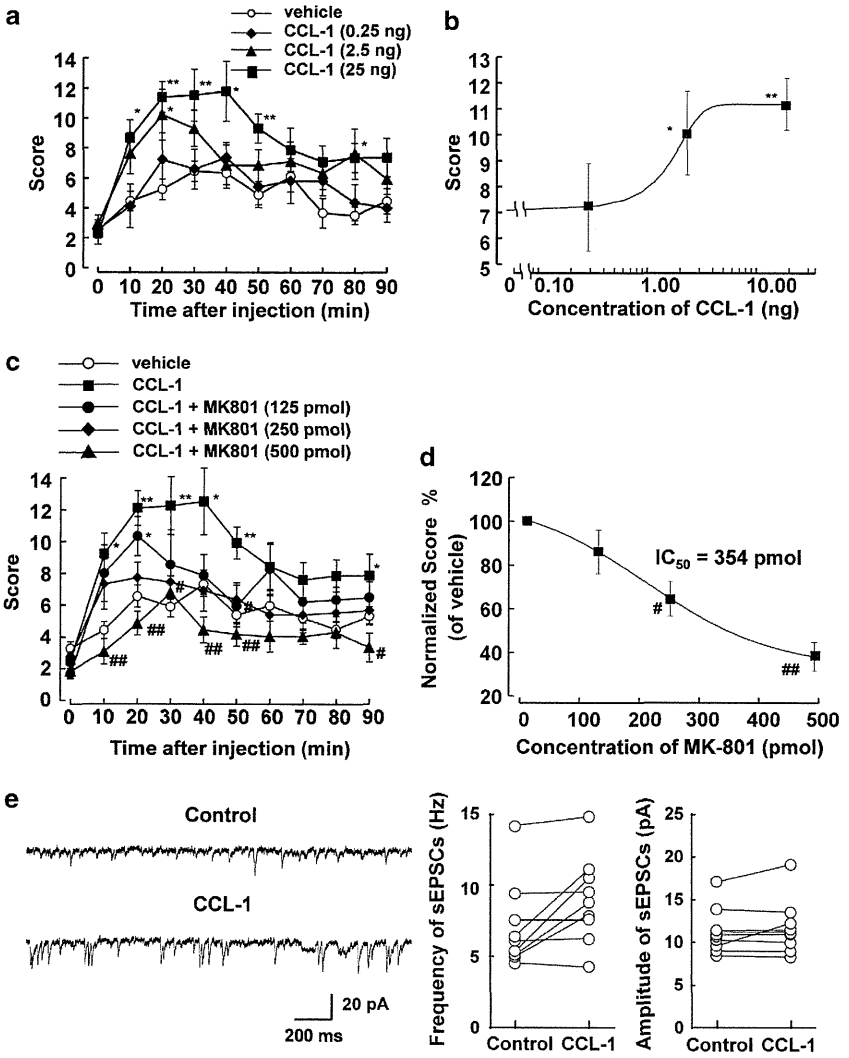

Figure 5 Induction of allodynia by CCL-1 and attenuation of CCL-1-induced allodynia by NMDA antagonist and effect of CCL-1 on excitatory synaptic transmission in the superficial spinal dorsal horn. (**a**) Intrathecal (i.t.) injection of CCL-1 to naive mice induced allodynia (vehicle, $n=12$; each concentration of CCL-1, $n=8$). (**b**) Concentration dependence of CCL-1-induced allodynia 20 min after i.t. injection of CCL-1. (**c**) Co-injection of MK-801 blocked allodynia induced by CCL-1 (25 ng, i.t.) (vehicle, $n=12$; each concentration of MK-801, $n=8$). (**d**) Concentration-dependent inhibition of allodynia by MK-801 50 min after injection. The concentration of MK-801 for 50% inhibition (IC_{50}) was 354 pmol. Data represent mean ± S.E. $^{**}P<0.01$, $^{*}P<0.05$ *versus* vehicle; $^{\#\#}P<0.01$, $^{\#}P<0.05$: *versus* CCL-1 (25 ng) (two-way analysis of variance followed by Tukey–Kramer tests). (**e**) Representative excitatory effect of CCL-1 (50 ng/ml) on sEPSCs evoked in substantia gelatinosa neurons at a holding potential of −70 mV (the left traces). CCL-1 elicited a barrage of sEPSCs. The excitatory action of CCL-1 was detected in about 40% of neurons tested (see Result section). Graphs in the right show CCL-1 actions on the frequency and amplitude of sEPSCs ($n=9$)

NR2B subunit at Tyr1472 (p-NR2B) in the spinal cord at 1 and 3 h after injection of CCL-1 (25 ng, i.t.) (relative protein levels, 2.4 ± 0.24, 4.7 ± 0.18, respectively; $n=3$; Figure 6f). After immunoblotting, the membrane was stripped and reprobed with anti-NR2B antibody (Figure 6b). CCL-1 increased level of NR2B protein at 1, 3 and 7 days after injection of CCL-1 (25 ng, i.t.; relative protein levels, 2.9 ± 0.33, 2.9 ± 0.35, 3.2 ± 0.65, respectively; $n=3$; Figure 6g). The protein level of p-NR2B/NR2B was increased at 1 and 3 h after injection of CCL-1 (25 ng, i.t.; relative protein levels, 0.90 ± 0.34, 0.97 ± 0.34, respectively; $n=3$; Figure 6h).

Effects of CCL-1 injection on glial cells and cytokines in the spinal cord. Activation of glial cells contributes to the development and maintenance of tactile allodynia.[11,13] We examined microglia and astrocytes in the spinal cord after injection of CCL-1 (25 ng, i.t.). Iba1 mRNA levels significantly increased in the spinal cord at 1, 3 h and 1 day after injection of CCL-1 (25 ng, i.t.; 179.8 ± 12.0, 168.4 ± 20.0, 149.5 ± 20.0%, respectively; $n=4$; Figure 7a). And we showed that CCL-1 (25 ng, i.t.) induced increase and morphological change of Iba1-positive microglia 1 day after injection (Supplementary Figure S3). CD11b mRNA levels also significantly increased in the spinal cord at 1 day after injection of CCL-1 (25 ng, i.t.; 249.5 ± 51.2%; $n=4$; Figure 7b). It was reported that $P2X_4R$ on microglia are important for the development of neuropathic pain.[2,3] We examined the expression of $P2X_4R$ mRNA after injection of CCL-1 (25 ng, i.t.). However, $P2X_4R$ mRNA had not changed after injection of CCL-1 (Figure 7c). Glial fibrillary acid protein

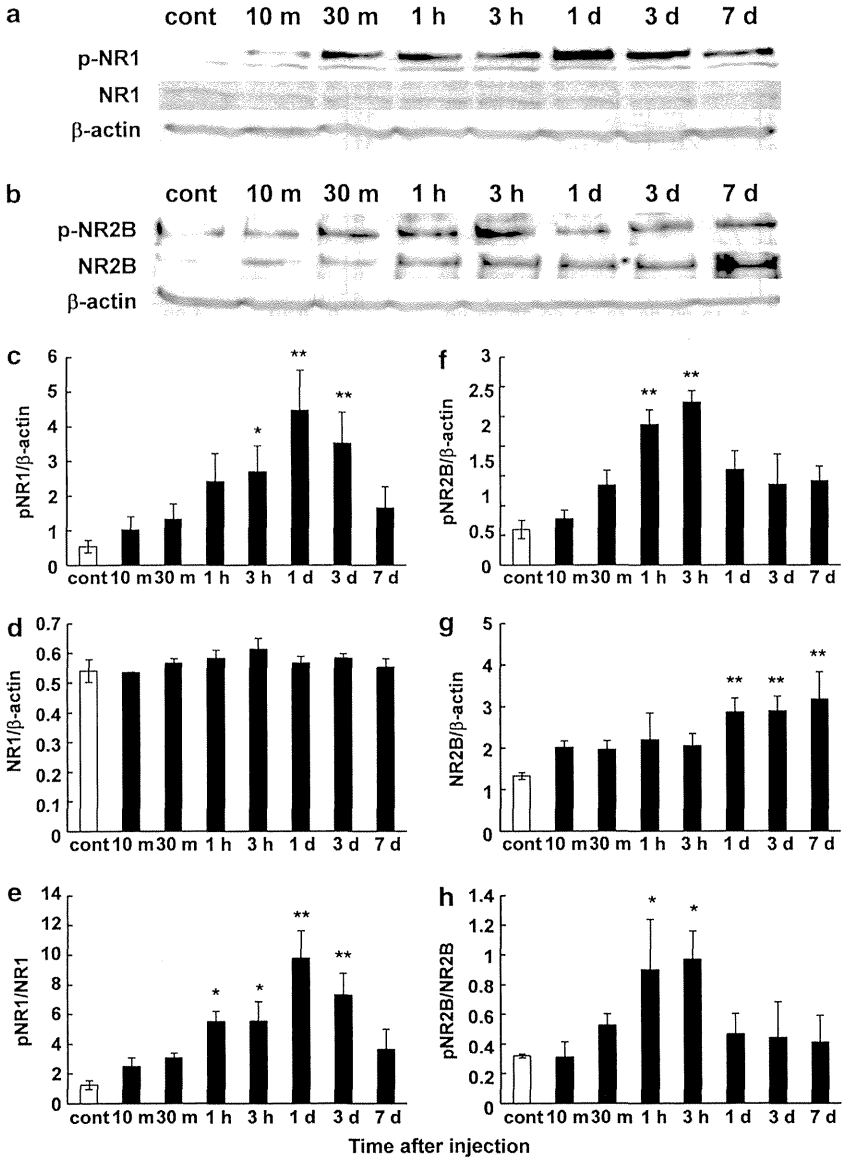

Figure 6 NMDAR phosphorylation after injection of CCL-1 in the spinal cord. (**a**) The phosphorylation levels of NR1 subunit at Ser896 (p-NR1) in the spinal cord at different time points after injection of CCL-1 (25 ng, i.t.) were evaluated by western blotting. The membrane was stripped and reprobed with anti-NR1 antibody. (**b**) The phosphorylation levels of NR2B subunit at Tyr1472 (p-NR2B) in the spinal cord at different time points after injection of CCL-1 (25 ng, i.t.) were evaluated by western blotting. The membrane was stripped and reprobed with anti-NR2B antibody. (**c**) The graph summarizes the protein level of p-NR1. (**d**) The graph summarizes the protein level of NR1. (**e**) Comparison of the levels of p-NR1 normalized to NR1. (**f**) The graph summarizes the protein level of p-NR2B. (**g**) The graph summarizes the protein level of NR2B. (**h**) Comparison of the levels of p-NR2B normalized to NR2B. Data represent mean ± S.E. ($n=3$). $^{**}P<0.01$, $^{*}P<0.05$: *versus* control (cont) (one-way analysis of variance followed by Bonferroni's test)

(GFAP) mRNA level significantly increased in the spinal cord at 1, 3 h and 1 day after injection of CCL-1 (25 ng, i.t.; 199.1 ± 19.0, 163.5 ± 16.6, 169.7 ± 20.8%, respectively; $n=4$; Figure 7d). In addition, we observed that CCL-1 (25 ng, i.t.) induced morphological change and the number of GFAP-positive astrocytes 1 day after injection (Supplementary Figure S3). Furthermore, we examined activation of microglia and astrocytes after injection of CCL-1 (25 ng, i.t.) using phosphor-p38 MAPK antibody (p-p38). CCL-1 induced phosphorylation of p38 MAPK on microglia and astrocytes (Supplementary Figure S2). Cytokines and growth factors are important mediators of neuronal–glial interactions.[12,23] We examined cytokine (IL-1β, TNF-α, IL-6) and brain-derived neutrophic factor (BDNF) in the spinal cord after injection of CCL-1 (25 ng, i.t.). Though protein levels of IL-1β, TNF-α and IL-6 were not changed after 7 days of nerve ligation (Figure 1b), IL-1β mRNA significantly increased in the spinal cord at 1 and 3 h after injection of CCL-1 (25 ng, i.t.; 688.0 ± 150.8, 609.2 ± 148.1%, respectively; $n=4$; Figure 7e), as well as TNF-α mRNA at 30 min, 1 and 3 h (25 ng, i.t.; 368.1 ± 150.1, 485.8 ± 94.4, 408.1 ± 97.4%, respectively; $n=4$; Figure 7f), and IL-6 mRNA at 1 and 3 h (25 ng, i.t.; 248.7 ± 40.8, 318.0 ± 68.8%, respectively; $n=4$; Figure 7g) after injection of CCL-1. On the other hand, BDNF mRNA did not change after injection of CCL-1 (Figure 7h).

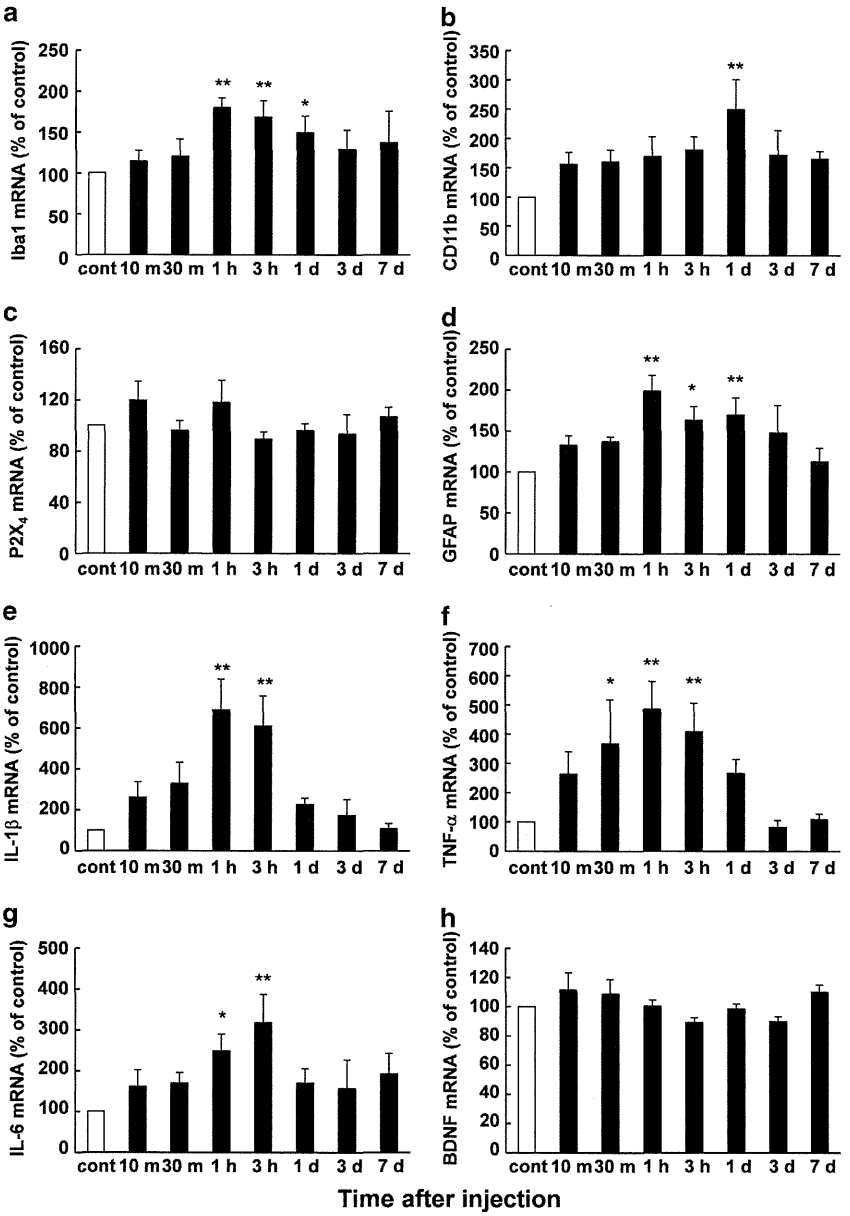

Figure 7 CCL-1 increased the expression of glial cells and cytokines in the spinal cord. Expression of mRNA of (**a**) Iba1, (**b**) CD11b, (**c**) $P2X_4R$, (**d**) GFAP, (**e**) IL-1β, (**f**) TNF-α, (**g**) IL-6 and (**h**) BDNF after injection of CCL-1 (25 ng, i.t.) were evaluated by RT-PCR. Each value was normalized to the control level (cont). Data represent mean ± S.E. ($n=4$). $^{**}P<0.01$, $^{*}P<0.05$: *versus* control (one-way analysis of variance followed by Bonferroni's test)

Effects of i.t. CCR-8 siRNA treatment on allodynia. We next examined the effects of CCR-8 downregulation on tactile allodynia. We made CCR-8 knockdown model using transfection of siRNA against CCR-8. We confirmed that protein level of CCR-8 was reduced in the spinal cord 5 days after injection of CCR-8 siRNA (Figure 8a). The CCR-8 knockdown mice were subjected to PSNL 5 days after injection of CCR-8 siRNA. We examined the effect of CCR-8 knockdown on allodynia and coordinated motion using von Frey filament test and rota-rod test. Downregulation of CCR-8 reduced PSNL-induced tactile allodynia for 2 weeks ($n=5$; Figure 8c). By contrast, downregulation of CCR-8 had no effect on coordinated motion ($n=5$; Figure 8d).

Discussion

The present study, for the first time, demonstrates that expression of CCL-1 in the spinal cord and DRG at the mRNA and protein levels is increased after nerve ligation, and the nerve ligation-induced tactile allodynia is attenuated by treatment with neutralizing antibody against CCL-1 and in CCR-8 knockdown mice. We further show that CCL-1 has an excitatory action on the glutamatergic synaptic transmission and phosphorylation of NMDAR subunits, NR1 and NR2B, in the spinal dorsal horn and increase expression of glial cells activation markers (Iba1, CD11b and GFAP) and cytokines (IL-1β, TNF-α and IL-6). Our results therefore indicate that CCL-1 may be one of the key mediators of chronic tactile

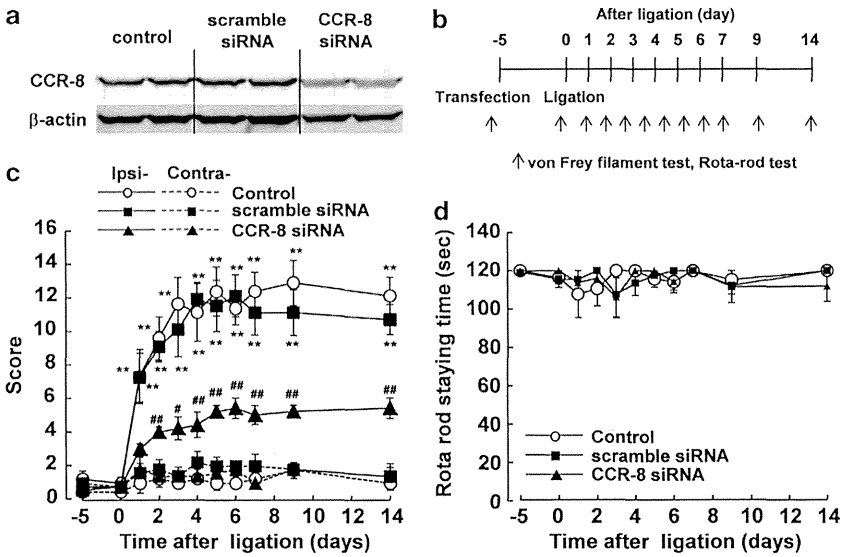

Figure 8 Intrathecal siRNA against CCR-8 treatment inhibited allodynia-induced nerve ligation. (**a**) Protein level of CCR-8 in the spinal cord after transfection of CCR-8 siRNA. (**b**) Schedule for making model mice and behavioural analysis. (**c**) CCR-8 siRNA inhibited allodynia-induced nerve ligation. (**d**) There was no change in coordinated motion after siRNA treatment. Data represent mean ± S.E. ($n=5$). $^{**}P<0.01$ *versus* contralateral; $^{\#\#}P<0.01$, $^{\#}P<0.05$: *versus* scramble siRNA (two-way analysis of variance followed by Tukey–Kramer tests)

allodynia acting through an acute modulation of nociceptive synaptic transmission, phosphorylation of NR1 and NR2B, glial activation and increase of cytokines in the spinal cord.

In this study, we showed that CCL-1-specific receptor, CCR-8, was expressed in not only neurons but also glial cells 6 h after nerve ligation in the ipsilateral side (see Figure 3). We suggested that increase of total CCR-8 protein after nerve ligation in the spinal cord by increase of CCR-8 expression on glial cells. CCL-1 mRNA showed only a transient increase in the spinal cord (see Figure 1e) and at 3 h, 1 and 3 days after nerve ligation in DRG (see Figure 1d). This indicates that CCL-1 may be mainly produced in DRG after nerve ligation. In the case of CCL-21 and CCL-2, they were produced in DRG after nerve ligation and were transported to neuronal terminals in the dorsal horn.[24,25] CCL-2 was released from neuronal synaptic vesicles in the spinal cord.[26] Similarly, we assume that CCL-1, which is produced in DRG neurons after nerve ligation, is subsequently transported to the spinal cord and then released. CCL-1 mRNA in the spinal cord at 3 h after nerve ligation was also produced in glial cells albeit only transiently; this however, requires further investigation.

Immune cells and glial cells interact with neurons to alter pain sensitivity and to mediate the transition from acute to chronic pain.[11,14,19] It is generally believed that microglia are involved in the development and astrocytes in the maintenance of neuropathic pain.[27–29] Cytokines are important messengers for the communication between neurons and glia.[11,13,30] Injection of CCL-1 into the spinal cord increased the mRNA level of microglial (CD11b or Iba1) and astroglial (GFAP) markers, as well as that of cytokines (IL-1β, TNF-α and IL-6) (see Figure 7). We also observed double staining of GFAP or CD11b with p-P38 after i.t. injection of CCL-1, suggesting that microglia and astrocytes were in reactive states (see Supplementary Figure S2). Activation of microglia in the spinal dorsal horn following peripheral nerve injury is well characterized.[2,31] The mechanisms of nerve injury-induced microglial activation are complex and involve several signaling systems.[32] Purinergic signaling mediated through $P2X_4$, $P2X_7$ and $P2Y_{12}$ receptors seems to contribute to the initial activation of microglia following acute nerve injury.[2,3,16,31,33,34] We, however, failed to identify changes in $P2X_4$ receptor mRNA in the spinal cord after injection of CCL-1. This suggests that CCL-1-mediated activation of microglia does not involve the upregulation of $P2X_4$ receptors but engages distinct signaling cascade(s). Several reports have previously demonstrated that cytokines and chemokines activate microglia and astrocytes, inducing secretion of proinflammatory factors (e.g., IL-1β, TNF-α, BDNF, IL-6, IL-17, CCL-2).[2,12,27] Several proinflammatory cytokines and chemokines have been implicated in altered nociceptive processing.[12] TNF-α enhanced synaptic efficacy by increasing surface expression of AMPA receptors.[35] IL-1β modulates sensory neuron transmission via increased release of the nociceptive neuropeptides substance P and calcitonin gene-related peptide.[36–38] IL-1β also induced the phosphorylation of NR1.[39] IL-6 was reported to be involved in the development of neuropathic pain.[40] By contrast, there are some reports that IL-6 has neuroprotective effect in the central nerve system.[41] IL-1β and TNF-α induced IL-6 expression in cultured neurons and astrocytes.[42] According to these reports, it might be reasonable that a peak expression of IL-6 in the spinal cord occurred later compared with that of TNF-α and IL-1β after injection of CCL-1 (see Figure 7g). These results indicate that CCL-1 is involved in the development of allodynia through glial activation and expression of cytokines. However, other signaling molecules can be also involved in the pathogenesis of neuropathic pain. Effects of CCL-1 on glial function need to be investigated in more detail in the future.

We showed that allodynia induced by injection of CCL-1 was blocked by co-injection of NMDAR antagonist.

We assumed that CCL-1 enhanced glutamate release from presynaptic terminal or affected postsynaptic NMDARs. We confirmed that CCL-1 affected both, increasing glutamate release transiently and inducing phosphorylation of NR1 and NR2B gradually. As for the presynaptic effect, we showed that CCL-1 increased glutamate release only in some but not all neurons (see Figure 5e). Similarly, double immunostaining with anti-CCR-8 and anti-NeuN showed that CCR-8 expression was only in sub-population of neurons (see Figure 3), the reason of which requires further investigation. As for the postsynaptic effect, it is already reported that activation of NMDAR is important for initiating long-lasting changes in synapses and has been implicated in persistent pain by strengthening glutamatergic sensory transmission.[5] Though we did not directly check whether postsynaptic NMDA currents were enhanced by CCL-1 or not, we observed that both phosphorylation of NMDAR and increase in the number of NMDARs take place in response to CCL-1. Phosphorylation of NMDAR is known to modulate NMDAR activity and facilitate transmission of nociceptive inputs in inflammatory and neuropathic pain models.[39] Partial ligation of sciatic nerve significantly increased the phosphorylated proportion of NR1 and NR2B subunits in the dorsal horn.[43,44] The phosphorylation of NR1 subunit is related to enhancement of synaptic efficacy and the development of central sensitization 7 days after nerve injury.[45] On the other hand, NR2B selective antagonist attenuated neuropathic pain.[46] Tyrosine phosphorylation of NR2B, but not NR2A, is associated with the development of persistent pain.[47] In our experiments, CCL-1 induced phosphorylation of NR1 and NR2B albeit with different time course: Phosphorylation of NR2B was transient, whereas phosphorylation of NR1 continued for 3 days. In our behavioural experiments on pain score, injection of CCL-1 induced allodynia transiently, as phosphorylation of NR2B. As there is a report that NR2B is particularly important for pain perception,[5] we speculate that phosphorylation of NR2B would be more important than phosphorylation of NR1 together with upregulation of NR2B. As for the phosphorylation of NR1, IL-1β was reported to induce phosphorylation of NR1.[45,48] As IL-1β mRNA was increased in the spinal cord after injection of CCL-1 at 1 and 3 h (Figure 7e), we speculate that NR1 would be phosphorylated not only by CCL-1 but also by IL-1β.

In conclusion, our study provides evidence that CCL-1 is produced mainly in DRG after nerve ligation, supposed to be transported to the spinal cord, where it increases glutamate release together with local upregulated CCL-1, and then activates glial cells and cytokine release. CCL-1 also induced phosphorylation of NMDAR subunits, NR1 and NR2B. Treatment with neutralizing antibody against CCL-1 and CCR-8 siRNA blocked nerve ligation-induced tactile allodynia. Therefore CCL-1 is one of the key molecules in pathogenesis of allodynia, and CCL-1/CCR-8 signaling system can be a potential target for drug development in the treatment for neuropathic pain.

Materials and Methods

Animals. Male ddY mice (20–30 g, Kyudo Co. Ltd., Tosu, Saga, Japan) were used. Mice were housed at 23 ± 2 °C with 12 h light: 12 h dark cycle (light on from 0700 to 1900 hours) and were given free access to commercial food and tap water. Experimental procedures were based on the Guidelines of the Committee for Animal Care and Use of Kyushu University, Fukuoka University and National Institute for Physiological Sciences.

Drugs. Recombinant mouse CCL-1 and neutralizing antibody CCL-1 were purchased from R&D Systems (Minneapolis, MN, USA). MK801 was purchased from Sigma Aldrich (St. Louis, MO, USA).

PSNL. The mice were anesthetized with an intraperitoneal (i.p.) injection of pentobarbital (65 mg/kg). A PSNL was produced by tying a tight ligature with a No. 8 nylon thread around approximately 1/3–1/2 the diameter of the sciatic nerve located on the left side (ipsilateral side) based on the Seltzer method.[49] On the right side (contralateral side), the nerve was exposed without ligation.

Behavioural analysis. Behavioural analysis was performed to assess the development of tactile allodynia in mice. Tactile allodynia was measured using a von Frey filament (North Coast Medical, Gilroy, CA, USA). Mice were placed in glass cages with a wire mesh bottom and allowed to habituate for at least 1 h. A von Frey filament with bending forces of 0.16 g (innocuous stimulation) was pressed perpendicularly against the plantar skin of a hind-paw. The paw withdrawal responses to the mechanical stimulus were evaluated by scoring as follows: 0, no response; 1, lifting the hind-paw within 3 s; 2, lifting the hind-paw over 3 s; and 3, immediate flinching or licking of the hind-paw. The stimulation of the same intensity was applied seven times to each hind-paw at several seconds intervals and the total served as the pain-related score (score) in the SNL model. The behavioural data were analyzed using Origin (Microcal software Inc., Sunnyvale, MA, USA) software to determine the IC_{50} values.

We performed a rota-rod (KN-75 Rota-rod, Natume, Japan) test to measure motor balance and coordination. Mice were pre-trained on rota-rod apparatus for 3 days and then tested on the accelerating rod in which the speed of the spindle was 10 r.p.m. Latency until fall was automatically recorded. To eliminate stress and fatigue, mice were given a maximum cutoff latency of 120 s.

Intrathecal injection. Intrathecal (i.t.) injection was performed using a 25-μl Hamilton syringe with a 28-gauge needle (Muranaka Medical Instruments co. LTD., Osaka, Japan), as described previously.[50,51] The needle was inserted into the intervertebral space of a conscious mouse between the lumbar 5 (L5) and 6 (L6) regions of the spinal cord. A reflexive flick of the tail was considered to be an indicator of the accuracy of each injection. A volume of 5 μl was used for the i.t. injections.

Immunohistochemical analyses. Mice were anesthetized by pentobarbital sodium (50 mg/kg, i.p.) and perfused transcardially with saline followed by 4% paraformaldehyde in 0.1 M phosphate-buffered saline (PBS; 80 mM Na_2HPO_4, 20 mM KH_2PO_4, 150 mM NaCl, pH 7.4). The L4–L6 segment of the lumbar spinal cord was removed, postfixed in the same fixative and placed in 20% sucrose solution for 24 h at 4 °C. Transverse L4–L6 spinal cord section (20 μm) were sliced by a HM 550 cryostat (Micro-edge Instruments Co., Tokyo, Japan) and incubated for 1 h at room temperature in 5% donkey serum (Jackson Immuno Research, West Grove, PA, USA). Then, the sections were incubated with the following: NeuN (1 : 200, Millipore, Bilerica, MA, USA), CCR-8 (1 : 500, Enzo, New York, NY, USA), Iba1 (ionized calcium-binding adapter molecule-1, 1 : 2000, Wako, Osaka, Japan), CD11b (1 : 500, Serotec, Oxford, UK), GFAP (1 : 800, Millipore) or p-p38 (phosphor-p38 MAPK, 1 : 100, Cell Signaling Technology, Danvers, MA, USA) for 24 h at 4 °C. The sections were incubated for 4 h at room temperature in the secondary antibody (IgG-conjugated Alexa Fluor 488 or 594, 1 : 1000, Molecular Probes, Eugene, OR, USA). Sections were mounted on coverslips with permafluor aqueous mounting medium (Thermo Scientific, Yokohama, Japan). The sections were analyzed using a fluorescence microscope (BZ9000, Keyence, Japan) and a confocal laser scanning microscope (LSM510META, Carl Zeiss, Hallbergmoos, Germany). In confocal imaging, we used a series of Z-stack images (images taken at multiple focal points of an objective lens through the z -axis) for 3D analysis of each slice.

Cytokine array. Mouse cytokine array kit was purchased from R & D Systems and was assessed as described previously.[52] The L4–L6 segment of the lumbar spinal cord was isolated and homogenized in the lysis buffer (10 mM Tris-HCl, 0.5 mM EDTA, 0.5 mM EGTA, 1% Triton X-100, pH 7.4) containing protease inhibitor cocktail (Sigma) and centrifuged at 15 000 r.p.m. for 20 min at 4 °C. Each